

The Gaia-ESO Survey: calibration strategy[★]

E. Pancino^{1,2}, C. Lardo³, G. Altavilla⁴, S. Marinoni^{5,2}, S. Ragaini⁴, G. Coccozza⁴, M. Bellazzini⁴, E. Sabbi⁶, M. Zoccali^{7,8}, P. Donati^{4,9}, U. Heiter¹⁰, S. E. Koposov¹¹, R. Blomme¹², T. Morel¹³, S. Simon-Díaz^{14,15}, A. Lobel¹², C. Soubiran¹⁶, J. Montalbán^{17,27}, M. Valentini¹⁸, A. R. Casey¹¹, S. Blanco-Cuaresma¹⁹, P. Jofré^{11,20}, C. C. Worley¹¹, L. Magrini¹, A. Hourihane¹¹, P. François^{21,39}, S. Feltzing²², G. Gilmore¹¹, S. Randich¹, M. Asplund²³, P. Bonifacio²¹, J. E. Drew²⁴, R. D. Jeffries²⁵, G. Micela²⁶, A. Vallenari²⁷, E. J. Alfaro²⁸, C. Allende Prieto^{14,15}, C. Babusiaux²¹, T. Bensby²², A. Bragaglia⁴, E. Flaccomio²⁶, N. Hambly²⁹, A. J. Korn¹⁰, A. C. Lanzafame^{30,34}, R. Smiljanic³¹, S. Van Eck³², N. A. Walton¹¹, A. Bayo³³, G. Carraro¹⁷, M. T. Costado²⁸, F. Damiani²⁶, B. Edvardsson¹⁰, E. Franciosini¹, A. Frasca³⁴, J. Lewis¹¹, L. Monaco³⁵, L. Morbidelli¹, L. Prisinzano²⁶, G. G. Sacco¹, L. Sbordone^{8,7,34}, S. G. Sousa³⁷, S. Zaggia²⁷, and A. Koch³⁸

(Affiliations can be found after the references)

Received September 15, 1996; accepted March 16, 1997

ABSTRACT

The Gaia-ESO survey (GES) is now in its fifth and last year of observations, and has already produced tens of thousands of high-quality spectra of stars in all Milky Way components. This paper presents the strategy behind the selection of astrophysical calibration targets, ensuring that all GES results on radial velocities, atmospheric parameters, and chemical abundance ratios will be both internally consistent and easily comparable with other literature results, especially from other large spectroscopic surveys and from Gaia. The calibration of GES is particularly delicate because of: (i) the large space of parameters covered by its targets, ranging from dwarfs to giants, from O to M stars, and with a large range of metallicities, as well as including fast rotators, emission line objects, stars affected by veiling and so on; (ii) the variety of observing setups, with different wavelength ranges and resolution; and (iii) the choice of analyzing the data with many different state-of-the-art methods, each stronger in a different region of the parameter space, which ensures a better understanding of systematic uncertainties. An overview of the GES calibration and homogenization strategy is also given, along with some examples of the usage and results of calibrators in GES iDR4 – the fourth internal GES data release, that will form the basis of the next GES public data release. The agreement between GES iDR4 recommended values and reference values for the calibrating objects are very satisfactory. The average offsets and spreads are generally compatible with the GES measurement errors, which in iDR4 data already meet the requirements set by the main GES scientific goals.

Key words. Surveys – Galaxy: general – Stars: abundances – Techniques: spectroscopic – Techniques: radial velocity

1. Introduction

The detailed study of the Milky Way (MW) as a galaxy has emerged as a central field in modern astrophysics and is currently attracting much attention, not the least thanks to the launch of the Gaia ESA space mission in December 2013 (Gaia Collaboration 2016a; Gaia Collaboration et al. 2016b; Lindegren & Perryman 1996; Mignard 2005; de Bruijne 2012). For in-depth studies of the properties of the stellar populations in the MW, high-multiplex spectroscopy of sufficient resolution is required to obtain radial velocities (RV), stellar astrophysical parameters (AP), and elemental abundances for large numbers of stars (Freeman & Bland-Hawthorn 2002; Bland-Hawthorn et al. 2010). Several new instruments have been designed around this idea (including HERMES, 4MOST, and WEAVE; Barden et al. 2010; de Jong et al. 2014; Balcells et al. 2010) and several spectroscopic surveys are ongoing or planned with this goal in mind (for example RAVE, APOGEE, GALAH, and LEGUE; Kordopatis et al. 2013; Majewski et al. 2015; De Silva et al. 2015; Newberg et al. 2012). All these surveys will study millions of stars, but

they will adopt different selection criteria, instrumental setups, and data analysis methods.

The Gaia-ESO public spectroscopic survey (GES, Gilmore et al. 2012; Randich et al. 2013) started operations at the end of 2011, with the goal of exploring all components of the MW in a complementary way to Gaia. GES uses the FLAMES optical spectrograph (Pasquini et al. 2000) at the ESO (European Southern Observatory) VLT (Very Large Telescope), in Medusa combined mode, where 6 to 8 fibers are used by UVES with a resolution of $R=\lambda/\Delta\lambda \approx 47\,000$, and 132 fibers are used by GIRAFFE, with $R \approx 16\,000$ – $25\,000$, depending on the wavelength range chosen (see Table 1 for a list of the GES observing setups used). GES is measuring RVs and derive APs and chemical abundances of several elements for $\sim 10^5$ stars, focussing on relatively faint stars (mainly $V > 16$ mag), for which Gaia will not be able to provide accurate RVs and abundances. GES data have their own outstanding scientific and legacy value, but together with the Gaia data they will provide extremely detailed 6D space information (position, distance, and 3D motions), combined with astrophysical information, for a representative sample of MW stars.

Stellar spectroscopic surveys require specific calibrators, to allow for meaningful comparisons with other literature studies

[★] Based on data products from observations made with ESO Telescopes at the La Silla Paranal Observatory under programme IDs 188.B-3002 and 193.B-0936.

Table 1. FLAMES instrumental setups used in the Gaia-ESO Survey, with the number of individual stars analysed in iDR4 for each setup. The official ESO setup data presented here refer to the period covered by GES iDR4 observations, i.e., before August 2014.

Instrument	Setup	λ_{\min} (Å)	λ_{\max} (Å)	R ($\lambda/\Delta\lambda$)	iDR4
UVES	520 ^{a,d}	4140	6210	47000	337
UVES	580 ^{b,d}	4760	6840	47000	3281
UVES	860 ^c	6600	10600	47000	—
GIRAFFE	HR3 ^{a,d}	4033	4201	24800	822
GIRAFFE	HR4 ^{a,e}	4188	4297	24000	—
GIRAFFE	HR5A ^{a,d}	4340	4587	18470	823
GIRAFFE	HR6 ^{a,d}	4538	4759	20350	806
GIRAFFE	HR9B ^d	5143	5356	25900	2243
GIRAFFE	HR10 ^f	5339	5619	19800	29215
GIRAFFE	HR14A ^{a,d}	6308	6701	17740	683
GIRAFFE	HR15N ^d	6470	6790	17000	19431
GIRAFFE	HR21 ^f	8484	9001	16200	31649

^(a)Mostly used for OBA stars (WG13).

^(b)Mostly used for FGK stars (WG10, WG11, WG12).

^(c)Used for benchmark stars (legacy value only, no analysis).

^(d)Used for OCs; HR09B is generally used for stars of type A and hotter, while HR15N is used for stars of type F and cooler.

^(e)Not in iDR4, introduced only recently.

^(f)Used for MW field stars.

and spectroscopic surveys, but also for internal homogenization purposes. GES has chosen to invest a significant effort on calibrations, because of the large variety of stellar targets, and consequently of observational setups and analysis methods. Of course, the calibration objects do not serve only to assess the internal consistency, but also to allow for external comparisons with other large surveys and with Gaia. This will maximize their legacy value and provide a rich reference dataset for future inter-survey calibrations.

In this paper we describe the GES calibration needs, the calibrating targets selection and observation processes, and the various uses and purposes of the chosen calibrators in the framework of the GES data analysis. We use the GES iDR4 data¹ to illustrate how the calibrators are employed in GES, and with which results. The paper is organized as follows: in Section 2 we discuss the general basis and implementation of the GES calibration strategy; the following sections discuss various types of calibrators like RV standards (Section 3); open and globular clusters (OC and GC, respectively, Section 5); benchmark stars (Section 4); astroseismologic constraints (Section 6). In Section 7 we present our summary and conclusions.

2. GES calibration needs and strategy

The broad scientific goal of GES is to survey all MW components, including the disk(s), the bulge, the halo, with special attention to the Solar neighborhood, that will be studied by Gaia in extreme detail (Gilmore et al. 2012). GES includes OCs of all ages, excluding only those that are still embedded (Randich et

¹ GES iDR4 is the fourth internal data release, where a large fraction of the data obtained before the end of August 2014 were re-analyzed homogeneously, taking into account the lessons learned in the previous internal releases. GES iDR4 will also form the basis of the next GES public data release through the ESO Phase3 portal for public surveys, which is expected in Autumn 2016.

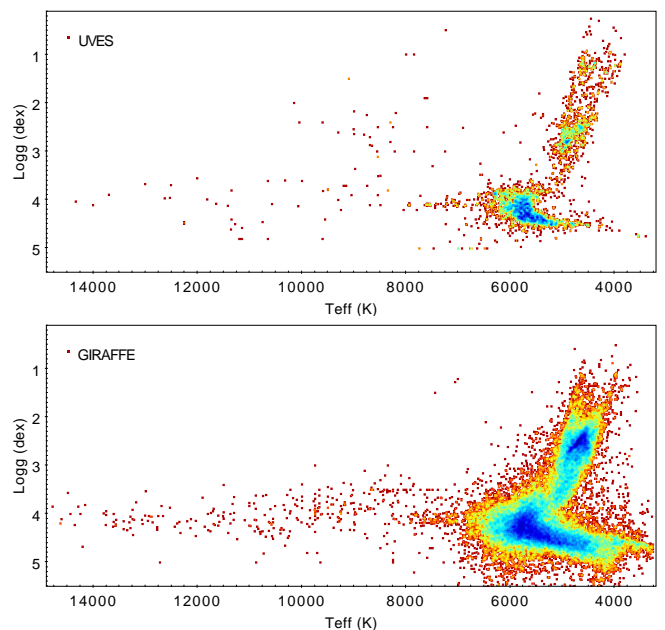


Fig. 1. Parameter coverage of GES iDR4 stars. The top panel shows stars observed with UVES and the bottom one with GIRAFFE. The color-scale refers to the density of points (red is low density while blue is high). A long tail of hot stars extending to $T_{\text{eff}} > 14\,000$ K was cut for plot readability.

al. 2013), to study their internal properties and evolution, and as tracers of the thin disk population.

As a result, GES targets cover a wide range of properties, from dwarfs to giants, from O to M stars, and with a wide range of metallicities and abundance patterns. Figure 1 shows the parameter space coverage of the 54 530 iDR4 GES targets for which recommended parameters² were produced. The corresponding [Fe/H] distribution is presented in Figure 2. *As a first obvious requirement, GES calibrators must cover adequately this wide range of properties.*

The analysis of the stellar spectra obtained by GES has been organized in a set of Working Groups (WGs). The characteristics of each WG are described in detail elsewhere, but in short: WG10 deals with the GIRAFFE analysis of FGK stars (Recio-Blanco et al., in preparation), WG11 with the UVES analysis of FGK stars (Smiljanic et al. 2014), WG12 with the analysis of pre-MS and of cool stars (Lanzafame et al. 2015), and WG13 with the analysis of hot stars (Blomme et al., in preparation). Within each WG, almost all of the state-of-the-art methodologies – appropriate for different objects – are implemented and applied by various research groups called *abundance analysis nodes*. They cover various methodologies, from full spectral synthesis to classical EW (Equivalent Width) techniques, and using a variety of abundance computation codes. Some are more suited to deal with specific stellar properties like for example stellar rotation or veiling. Others were designed for accurate measurements of specific features, for example lithium or the H_α line. More details on the individual nodes abundance analysis methods can be found in the above cited papers, describing the WG analysis. This is a major strength of GES, because it allows for method intercomparisons that are extremely instructive on the strengths, weaknesses and applicability ranges of each method,

² Here and in the rest of the paper, the *recommended* values, APs, RVs, or abundances are the final values produced by GES after the whole homogenization procedure.

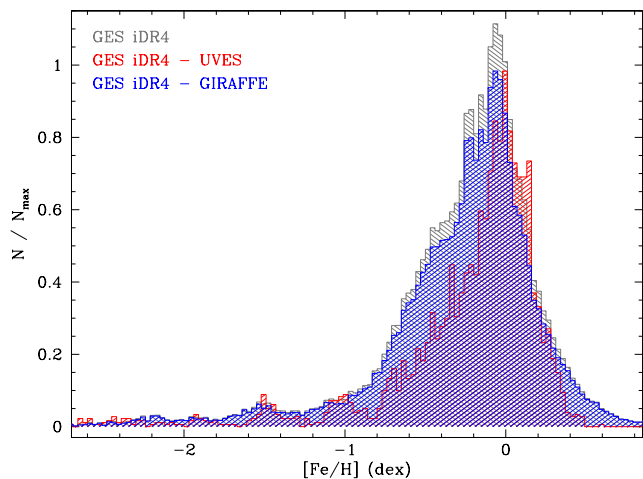


Fig. 2. Metallicity distribution of GES iDR4 targets as a whole (grey-shaded histogram), and of the UVES (red-shaded) and GIRAFFE (blue-shaded) targets in iDR4. The histogram of the whole sample was normalized differently for clarity.

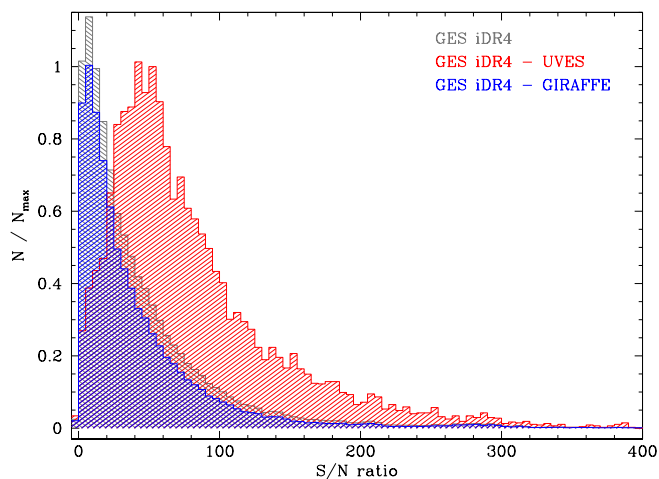


Fig. 3. Histogram of the S/N ratio distribution for individual spectra in GES iDR4 (grey-shaded histogram), and of UVES (red-shaded) and GIRAFFE (blue-shaded) individual spectra. The whole iDR4 sample is normalized differently for clarity.

and for a deep knowledge of systematic errors. However, this complexity of the data analysis places another strong requirement on the calibration strategy: *that an adequate number of calibrating objects fall also into those regions of the parameter space that are analyzed by more than one WG and node.*

Finally, as a natural consequence of the large variety of science targets and methods, the observing strategy relies on several different observing setups, that are appropriate for different types of objects and are summarized in Table 1. Also, depending on the science goal (focus on RVs or on chemical abundances), a wide range of S/N ratios were obtained, as shown in Figure 3. This places another requirement on GES calibrations: *an adequate number of (calibrating) objects need to be observed with more than one setup and with a range of S/N ratios.*

All the calibration requirements described above ensure that GES is both internally consistent with respect to the different methods, objects, and observational setups, and easily comparable with other literature results. Therefore, a good fraction of

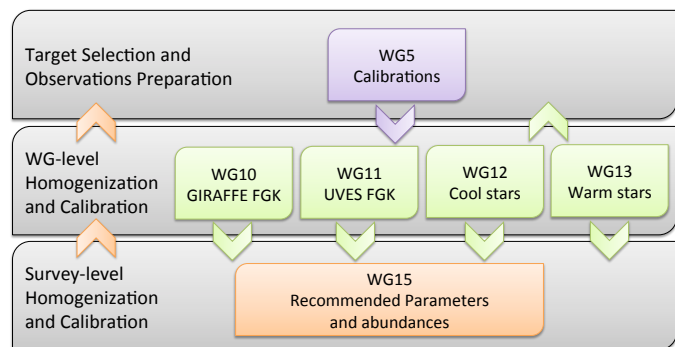


Fig. 4. The iterative GES calibration and homogenisation process. Arrows mark the flow of information from target selection (described in this paper), to abundance analysis, and production of recommended parameters and abundances. Between and during abundance analysis cycles, feedback is provided by the downstream layers, to refine both the calibration observations and the analysis strategy. Only those WGs that make use of calibrators are indicated in this figure.

the calibrators need to be well studied objects with reliable reference parameters and abundances. It is also desirable that some of the calibrators are observed by other large surveys as well, to enhance the legacy value of GES. The ensemble of all the internal and external calibration procedures in GES is referred to as *homogenisation*.

2.1. GES analysis workflow

GES data analysis proceeds in cycles, also called internal data releases (iDR). Within each cycle, the survey calibration and homogenisation is organized in three logical layers, as illustrated in Figure 4. The starting one, coordinated by WG5, takes care of selecting the appropriate calibrating objects and of preparing their observations, which is the main topic of the present paper. In a second layer, appropriate calibrators are used by the WGs to compare and combine the node-level APs and abundances into WG-level recommended parameters. Finally, in different stages along each cycle, WG15 performs a homogenisation of the WG-level results, to provide survey-level recommended RVs, APs, and chemical abundance ratios.

Internal consistency among abundance analysis nodes is facilitated as much as possible³ by the use of a common set of atmospheric models (MARCS, see, Gustafsson et al. 2008), a common linelist (Heiter et al. 2015a), and a common grid of synthetic spectra, based upon the one by de Laverny et al. (2012). For the first processing cycles, up to iDR3, the homogenisation was carried out in a limited, exploratory way, based mostly on benchmark stars. During iDR4, the first full homogenisation took place at all levels, making use of all the observed calibrators and of new homogenisation algorithms. This effort provided important feedback on the calibration strategy, finalizing the calibrators selection strategy and the planning of the remaining calibration observations. The detailed homogenization procedure and algorithms are described in a companion paper (Hourihane et al., in preparation, hereafter H17).

³ This was not possible in all cases; for example, the hot stars abundance nodes obviously relied on a different set of atmospheric models.

2.2. GES calibrator types and observing strategy

The GES calibrators fall into a few main groups, described more in detail in dedicated sections, summarized here below. The list of iDR4 calibrators used in this paper is in Table 2.

- *Basic calibrations* in GES are mostly related to RV standard star observations, as described in Section 3.
- In GES, we extend the set of calibrating objects by including also *benchmark stars*, and in particular the Gaia FGK benchmark stars (Heiter et al. 2015b). They are carefully selected, well-studied stars, for which T_{eff} and $\log g$ were derived as independently from spectroscopy as possible (i.e., based on interferometric diameters, parallaxes, and so on, see Section 4 for more details). As such, they are good *absolute calibrators* of the parameters (i.e., for the accuracy), and useful references for the abundances.
- Like many other spectroscopic surveys, GES observes many stars belonging to OCs and GCs, as described more in detail in Section 5. These calibrators are quite powerful for checking the internal consistency of the abundance analysis (i.e., for the precision), as well as providing a relatively robust external reference for the abundance scale and AP determination.
- Collaborations are also ongoing with the CoRoT and Kepler teams, to obtain accurate $\log g$ reference values for large samples of giant stars, as described in Section 6.

The general idea behind the observing strategy is the following. For *internal* calibrations, each object should be observed with all the setups used by the different groups that will attempt a meaningful analysis of that object. For example, calibrators that can be in principle analysed by both OBA and FGK star experts should be observed with the setups adopted in GES for OBA stars (HR3, HR4⁴, HR5, HR6, and HR14) and FGK stars (HR9B, HR10, HR15N, HR21). In another example, OCs contain stars with properties overlapping those of the MW field part of the survey. To ensure that both OCs and field stars are analyzed consistently, a set of calibrating OCs should be observed with both the cluster (HR9B and HR15N) and the field (HR10 and HR21) GIRAFFE setups. More details on the typically adopted setups for each calibration type can be found in the following sections and in Table 1.

To minimize the impact on the total observing time assigned by ESO, calibration observations are carried out as much as possible in twilight. This is generally appropriate for the brightest objects. Wavelength calibration lamps are switched on during GIRAFFE observations for RV standards, while the usual GES procedure of inserting short exposures with the lamps on is employed for benchmarks and cluster observations, to avoid spoiling scientific exposures with scattered light from lamps.

All calibration data are reduced in the same way as any other GES observation to extract the final science-ready spectra. The ESO processing pipelines (Ballester et al. 2000) are employed to produce extracted and wavelength-calibrated UVES spectra, while a dedicated pipeline for the GIRAFFE processing was developed at CASU⁵ (Cambridge Astronomy Survey Unit). Both pipelines are complemented with GES-specific software to perform additional operations like sky subtraction or continuum normalization, radial velocity determination, and so on (for more details, see Jeffries et al. 2014; Sacco et al. 2014, for GIRAFFE and UVES, respectively).

⁴ This setup was introduced later to improve the $\log g$ determination for hot stars, so it was not employed for iDR4.

⁵ <http://www.ast.cam.ac.uk/mike/casu/>

Table 2. List of GES iDR4 calibrators used in this paper. The list is published in its entirety in the electronic version of the paper, and at CDS. It can be used to select the iDR4 calibrators from the upcoming ESO Phase 3 public release. Here we show a portion to illustrate its contents. The columns contain: (1) the GES unique identifier of each star (the CNAME), based on the object sexagesimal coordinates; (2) the calibration type, that can be GC or OC for clusters, RV for radial velocity standards, BM for benchmark stars, or CR for CoRoT targets; (3) the field name; (4) and (5) the 2MASS J and K magnitudes, when available.

CNAME	Type	Field	J (mag)	K (mag)
19250371+0049014	CR	Corot	11.27	10.47
21295872+1208321	GC	M15	11.78	11.39
11091266-5837236	OC	NGC3532	11.63	11.32
07391749+0513163	BM	Procyon	-9.99	-9.99
ssssssss-ssssssss	BM	Sun	-9.99	-9.99
21534196-2840169	RV	HIP108065	-9.99	-9.99

3. Basic calibrators

Basic spectroscopic calibrations generally include — besides the acquisition of an adequate set of calibration frames like bias, flat fields, wavelength calibration lamps, sky fibers placement⁶, and the like — the observation of *flux standard stars*, *radial velocity standard stars*, and hot, fast rotating stars for telluric absorption band removal, also referred to as *telluric standard stars*.

For a large spectroscopic survey like GES, where the main deliverables are chemical abundances, RVs, and APs, the flux calibration of spectra is not a crucial requirement and thus it is not performed. The correction for telluric absorption features is likewise not crucial, especially because it only affects the very last portion of HR21 GIRAFFE spectra, and short wavelength intervals in the UVES spectra⁷. If it will become necessary for specific scientific applications, telluric absorption bands can be efficiently removed, in future GES releases, with the use of Earth atmospheric models (for example, from the TAPAS collaboration, Bertaux et al. 2014). Therefore, no observations of telluric standards were carried out over the current survey, and none are overall planned.

Accurate and precise RV measurements are one of the main tools to fulfil the scientific goals of GES, and thus a specific calibration strategy was implemented.

3.1. Radial velocity standard stars

GES requires radial velocities with a precision in the range 0.3–1.0 km s⁻¹ to fulfil its various scientific goals (Gilmore et al. 2012), and both UVES and GIRAFFE have the potential of delivering RVs with a precision well below 500 m s⁻¹ (see also Sacco et al. 2014; Jackson et al. 2015). To reach an accuracy comparable to the quoted precision, it is necessary to keep the systematics under control, especially those related to the wavelength calibration scale, the non-uniform fiber/slit illumination, and the template mismatch in the cross-correlation procedure.

⁶ For young clusters or objects where the sky is expected to vary significantly across the FLAMES field of view, the sky fibers positioning and sky subtraction method are crucial.

⁷ Some key diagnostics, like the forbidden oxygen line at 6300 Å, are indeed affected by telluric absorption, and therefore we anticipate that a correction for telluric bands will be necessary for a detailed study of those diagnostics.

Table 3. Radial Velocity standards for zero-point calibration of GES, with their references RV measurements, taken from Soubiran et al. (2013) except for GJ 388 (Chubak et al. 2012).

ID	Type	V (mag)	RV (km/s)	δRV (km/s)
GJ 388	M4.5	9.43	12.453	0.066
HIP 616	K0V	8.70	-42.994	0.009
HIP 5176	G0	8.15	10.366	0.006
HIP 85295	K7V	7.54	-23.422	0.016
HIP 17147	F9V	6.68	120.400	0.007
HIP 20616	G0	8.41	38.588	0.009
HIP 26335	K7	8.78	21.772	0.006
HIP 26973	K0V	8.52	26.600	0.006
HIP 29295	M1/M2V	8.15	4.892	0.009
HIP 31415	F6V	7.70	-7.479	0.012
HIP 32045	K5	8.49	40.722	0.007
HIP 32103	G5/G6IV/V	8.53	27.167	0.006
HIP 33582	G0	9.02	-94.239	0.006
HIP 38747	G5	8.37	-8.002	0.007
HIP 45283	G2V	8.01	39.451	0.005
HIP 47513	M2	10.38	11.626	0.007
HIP 47681	G5V	8.41	11.289	0.007
HIP 50139	G1V	7.75	-21.976	0.005
HIP 51007	M0	10.15	21.758	0.006
HIP 58345	K4V	6.99	48.605	0.009
HIP 65859	M1V	9.05	14.386	0.009
HIP 66032	K2IV/Vp...	9.17	4.126	0.009
HIP 77348	G5	8.05	1.907	0.011
HIP 80423	G3/G5Vw...	9.32	-42.148	0.006
HIP 85295	K7V	7.54	-23.422	0.016
HIP 93373	G8V	8.60	-91.911	0.006
HIP 104318	G5	8.01	4.910	0.006
HIP 105439	K0 III+...	6.75	17.322	0.006
HIP 106147	K4/K5V	9.11	-84.533	0.009
HIP 108065	K0/K1III+.	7.82	-41.660	0.010
HIP 113576	K5/M0V	7.88	16.138	0.010

For GIRAFFE, to greatly reduce the systematics associated with the wavelength calibration, it was sufficient to associate to the scientific exposures short adjacent exposures with the SIMCAL (the simultaneous wavelength calibration lamp) switched on. Also the use of sky-lines can improve the RV accuracy, as shown by Jeffries et al. (2006) and Koposov et al. (2011). To reach an even better accuracy, below $\approx 300 \text{ m s}^{-1}$, the repeated observation of RV standards of different spectral types with the specific purpose of calibrating the RV zero point is necessary. For UVES, the use of sky lines has proved to reach a sufficient zero-point accuracy, thus no more UVES observations of RV standards were required starting from 2015, while for GIRAFFE they are continuing. More details on the wavelength and RV calibration strategy for GIRAFFE and UVES spectra, respectively, can be found in Jeffries et al. (2014), Sacco et al. (2014), and in the GES description papers (Gilmore et al.; Randich et al., in preparation).

GES was conceived to achieve its maximum impact once combined with Gaia data (Section 1), therefore the main source of RV standards for GES was the Gaia standard stars catalogue (Soubiran et al. 2013), complemented by Chubak et al. (2012). We relied on the best RV calibrators found in the Gaia catalogue, that appeared to be stable in RV within a few m s^{-1} over the explored time baseline (see Table 3 for a list of targets). Later, after the processing of the first internal data release (iDR1), the need

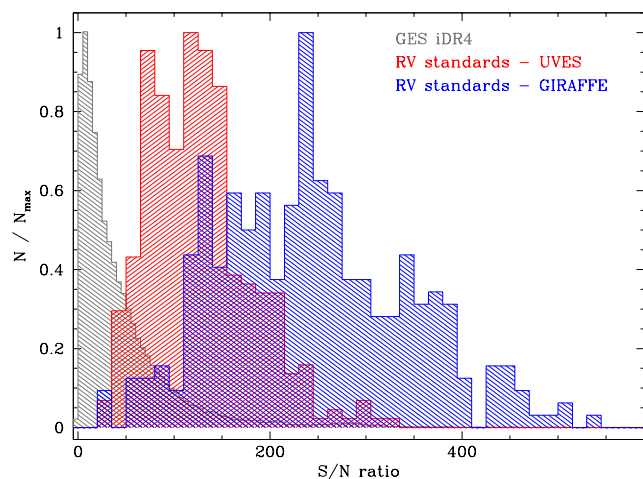


Fig. 5. S/N ratios of individual spectra of RV standards for the RV zero point calibration. There are between 2 and 20 spectra per star, typically 10. The UVES setup used is 580 (see Table 1) and the GIRAFFE setups are HR9B, HR10, 15N, and 21. The very high S/N ratios are due to the RV standards brightness (see Table 3) and to the need of integrating for relatively long exposure times, to average out illumination non-homogeneities within the fibres.

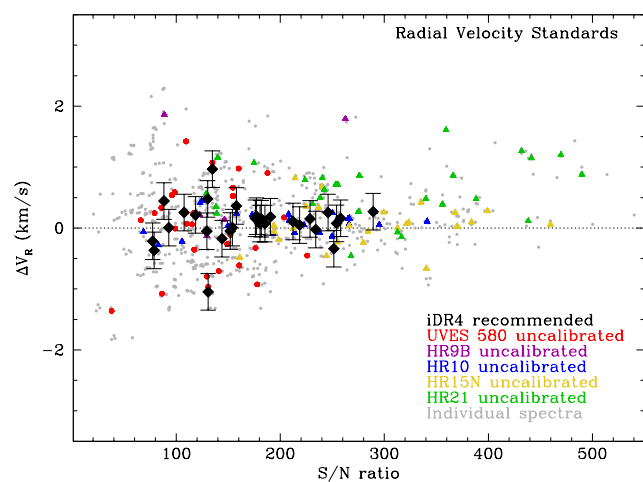


Fig. 6. Example of the result of RV homogenization on RV standards. Grey dots show the difference between individual spectra measurements and the reference values of Table 3. The coloured symbols are the same RV differences, but aggregated for each RV standard star in the various setups, and are still uncalibrated. The final iDR4 recommended values, obtained from the internal homogenization process, are shown by large black diamonds, which are placed at the average S/N ratio of the spectra obtained for each RV standard star.

for more RV stars cooler than $\approx 4000 \text{ K}$ emerged, and four M stars were included into the list. No hot standards are included in the calibration set. We are observing one or two RV standards in every observing run (approximately once per month). We used relatively long exposure times (about 100 s) compared to other bright calibrators like benchmark stars, avoiding saturation, not only to increase the S/N ratio (see Figure 5), but also to ensure uniform slit illumination, and with the SIMCAL on when observing with GIRAFFE.

Besides being used to set the zero-point of GIRAFFE RV measurements, the RV standards are also used in the WG15 ho-

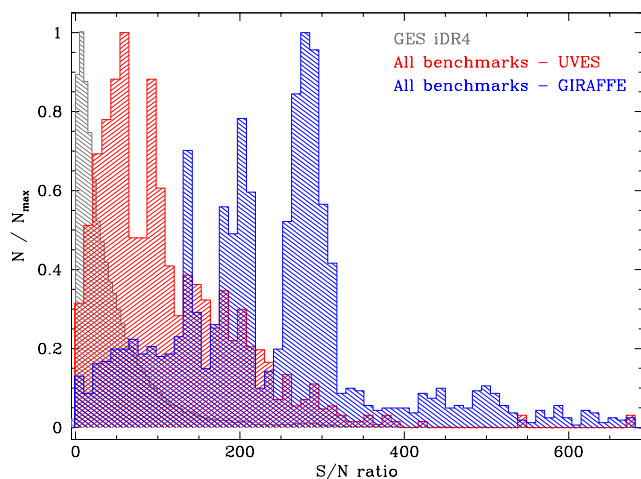


Fig. 7. S/N ratio of individual spectra of benchmark stars. In an initial phase, spectra were obtained in a range of S/N ratio values. Later, we aimed at obtaining at least 3 exposures per benchmarks star per setup, with a combined S/N > 100 per pixel (without saturating).

mogenization procedure, described in detail by H17. Briefly, the performance of each of the observed setups was tested with RV standards (see Figure 6), to identify the setups that show the smallest offset with respect to the reference values of Table 3. All other setups were corrected to the scale of the best setup (generally HR10, followed by HR15N) using the stars in common with the best available setup to compute an offset. In previous GES releases, offsets of $\approx 0.5 \text{ km s}^{-1}$ were reported between UVES and GIRAFFE (see Sacco et al. 2014; Donati et al. 2014; Lardo et al. 2015, among others). In iDR4, the two instruments showed much smaller differences, of a few meters per second, thanks to the use of sky lines to correct for UVES wavelength calibration uncertainties. The setup that shows the largest offset is HR21 ($\approx 0.5 \text{ km s}^{-1}$), for which the SIMCAL lamps are switched off to avoid contaminating the scientific exposure given the high efficiency of this particular setup.

4. Benchmark stars

In traditional works of stellar abundance analysis, the Sun is used as a reference, either to verify a posteriori the validity of the presented results by performing an analysis of a Solar spectrum with the same technique employed on the programme stars or to perform a differential analysis of the programme stars with respect to the Sun (see Sousa et al. 2014, for a GES-related example of this type of analysis). A second example of a reference star widely used for testing abundance analysis of cooler, more metal-poor stars is Arcturus (see, e.g., Ramírez & Allende Prieto 2011; Mészáros et al. 2013; Morel et al. 2014, and included references). Moreover, when large samples are analyzed, the stars in common among different literature studies are used as a comparison to put all data on the same system, as much as possible (see, e.g., Worley et al. 2012; De Pascale et al. 2014; Bensby et al. 2014). Within the Gaia mission preparatory effort, the concept of one reference star for APs determination and abundance analysis verification has been extended to define the so-called *Gaia benchmark stars* set (Heiter et al. 2015b). Benchmark stars ideally have known Hipparcos parallaxes, angular diameters, and bolometric fluxes, and their masses have been determined in a homogeneous way, so their effective temperatures and surface

Table 4. Gaia FGK benchmark stars observed in GES. Magnitudes and APs are from Heiter et al. (2015b), NLTE-corrected metallicities from Jofré et al. (2014).

ID	Type	V (mag)	[Fe/H] _{NLTE} (dex)	T _{eff} (K)	logg (dex)
Procyon	F5IV-V	0.366	+0.01	6545	4.00
HD 84937	sdF5	8.324	-2.03	6275	4.06
HD 49933	F2V	5.762	-0.41	6635	4.21
δ Eri	K1III-IV	3.527	+0.06	5045	3.76
HD 140283	sdF3	7.210	-2.36	5720	3.67
ϵ For	K2V	5.883	-0.60	5069	3.45
η Boo	G0IV	2.681	+0.32	6105	3.79
β Hyi	G0V	2.797	-0.04	5873	3.98
α Cen A	G2V	0.002	+0.26	5847	4.31
HD 22879	F9V	6.689	-0.86	5786	4.23
Sun	G2V	-26.74	0.00	5771	4.44
τ Cet	G8.5V	3.495	-0.49	5331	4.44
α Cen B	K1V	1.357	+0.22	5260	4.54
18 Sco	G2Va	5.505	+0.03	5747	4.43
μ Ara	G3IV-V	5.131	+0.35	5845	4.27
β Vir	F9V	3.608	+0.24	6083	4.08
Arcturus	K1.5III	-0.051	-0.52	4247	1.60
HD 122563	F8IV	6.200	-2.64	4587	1.61
ϵ Vir	G8III	2.828	+0.15	4983	2.77
ξ Hya	G7III	3.541	+0.16	5044	2.87
α Tau	K5III	0.867	-0.37	3927	1.22
ψ Phe	M4III	4.404	-1.24	3472	0.62
γ Sge	M0III	3.476	-0.17	3807	1.05
α Cet	M1.5IIIa	2.526	-0.45	3796	0.91
β Ara ^a	K3Ib-II	2.842	-0.05	4197	1.05
HD 220009 ^a	K2III	5.047	-0.74	4217	1.43
HD 107328	K0IIIb	4.970	-0.33	4496	2.09
ϵ Eri	K2Vk:	3.726	-0.09	5050	4.60

^aNot recommended as benchmarks from iDR5 on.

gravities can be derived as independently as possible from spectroscopy.

Even if FLAMES is not the ideal instrument to observe individual stars, it was deemed extremely important to observe these fundamental reference objects within GES. Being bright stars, they were observed mainly during twilight, with the three GES UVES setups and with the GIRAFFE HR9B, 10, 15N, and 21 setups (see Table 1), i.e., the four GES setups used for FGK stars in the MW field and in OCs. GES further extended the list to include also a few cooler K and M benchmarks and a few hotter O, B, and A benchmarks, as detailed in the next sections. The hot benchmark stars were observed also with the GES hot stars GIRAFFE setups: HR3, 5A, 6, and 14A (see Table 1). The S/N ratio of the observed spectra is reported in Figure 7.

Benchmark stars and candidate benchmarks are used both in the WG-level and survey-level homogenization processes, to assess which abundance analysis nodes and WGs, respectively, perform better in different regions of the parameters space, as expanded in Section 4.4. More details on the use of benchmark stars can be found in Smiljanic et al. (2014), Lanzafame et al. (2015), and H17.

4.1. Gaia FGK benchmarks

The FGK benchmark stars that were selected as GES astrophysical calibrators are listed in Table 4. They are extracted from the original set of Gaia FGK benchmark stars (Heiter et al. 2015b),

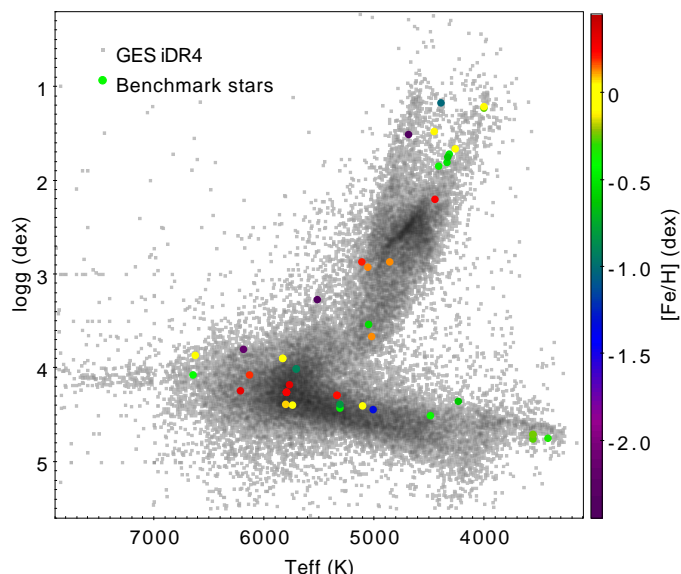


Fig. 8. Position on the T_{eff} - $\log g$ plane of the Gaia FGK benchmark stars (Heiter et al. 2015b, see also Section 4.1) analyzed in iDR4, coloured according to their $[\text{Fe}/\text{H}]$. A few of the cooler benchmarks ($T_{\text{eff}} < 4000$ K) described in Section 4.2 were also analyzed in iDR4. The whole GES iDR4 sample is reported in the background as smaller grey squares.

which contains 34 stars with T_{eff} in the range ≈ 3500 – 6500 K, $\log g$ in ≈ 0.5 – 4.5 dex, and with a metallicity ranging from super-solar to -2.5 dex. Additional spectra of these stars were gathered from the ESO archive (UVES and HARPS) and from the NARVAL archival observations at the Pic du Midi, and homogenized into a comprehensive library of high-resolution spectra (Blanco-Cuaresma et al. 2014). The only fundamental parameter that was not well constrained for these stars in the literature was $[\text{Fe}/\text{H}]$, thus an effort from the GES abundance analysis nodes was made to derive independently a set of reference $[\text{Fe}/\text{H}]$ value for each of them (Jofré et al. 2014, 2015), along with abundances for 10 elements, as a first step. Figure 8 gives an idea of the parameter space covered by the Gaia benchmark stars. The set only contains few metal-poor stars, a regime that is not much sampled in GES (see Figure 2), but we recently identified a few more candidates with $[\text{Fe}/\text{H}] < -1.2$ dex (Hawkins et al. 2016).

4.2. Additional M benchmarks

The collection of Gaia benchmark stars, from which we selected the sample described in the previous section, does not include a sufficient number of stars cooler than ≈ 3500 K. Benchmark stars in the M-dwarf region are needed both for Gaia (expected to observe more than one million M dwarfs) and GES, where M dwarfs are included among OC target stars. Angular diameter measurements for potential cool benchmark stars have only recently started to become available, and homogeneous metallicity determinations for the most promising ones are not available yet.

Nevertheless, we selected a number of candidate benchmarks among the best studied M-dwarf stars, listed in Table 5. For four of these stars, angular diameters were published by Boyajian et al. (2012) with a precision of 1–2%, while the angular diameters of GJ 436 and GJ 581 were determined by von Braun et al. (2011, 2012) to 3%, and that of GJ 551 by Demory et al. (2009) to 5%. Bolometric fluxes were measured for all stars by Boyajian et al. (2012) with a precision of 1%. These data give T_{eff} inde-

Table 5. Additional M-dwarf benchmark stars, with their magnitudes and spectral type from SIMBAD, metallicities as noted, and T_{eff} from Boyajian et al. (2012).

ID	Type	V (mag)	$[\text{Fe}/\text{H}]$ (dex)	T_{eff} (K)	Status
GJ 205	M1.5V	7.97	+0.35 ^a	3801	iDR3
GJ 436	M3V	10.59	+0.03 ^b	3416	iDR4
GJ 526	M1.5V	8.50	-0.30 ^a	3618	iDR4
GJ 551 ^c	M5.5V	11.05	+0.24 ^d	3054	—
GJ 581	M2.5V	10.61	-0.02 ^b	3442	iDR4
GJ 699	M4V	9.51	-0.39 ^a	3224	iDR3
GJ 880	M1.5V	8.64	+0.03 ^e	3713	iDR2

^aMetallicity from Rojas-Ayala et al. (2012).

^bMetallicity from Lindgren et al. (2016).

^cNot observed yet, we will rely on UVES archival data.

^dMetallicity from Jofré et al. (2014), considering α Cen A and B.

^eMetallicity from Neves et al. (2014).

pendent from photometry or spectroscopy for all stars, as listed in Table 5. Spectroscopic metallicity determination is more difficult for M dwarfs than for FGK dwarfs due to the more complex optical spectra. Several approaches have been pursued in the literature. These include calibrations of photometric data or low-resolution infrared spectroscopic features (e.g., Rojas-Ayala et al. 2012), or analysis of high-resolution spectra in optical or infrared regions (e.g., Önehag et al. 2012; Neves et al. 2014; Lindgren et al. 2016). Usually, samples of binaries with M- and FGK components are used for calibration or validation of the methods. Selected metallicities from various sources are listed in Table 5.

For most of these stars, there are additional high-resolution spectra available, in addition to those obtained with the GES setups. GJ 436, GJ 526, and GJ 880 were observed at optical and near-IR wavelengths with the NARVAL spectrograph. For GJ 436, GJ 551, GJ 581, and GJ 880, J-band spectra with $R=50000$ were obtained with the CRIRES spectrograph at the VLT. GJ 699 is included in the CRIRES-POP library (wavelength range from 1 to $5 \mu\text{m}$, Lebzelter et al. 2012). These high-quality archival data constitute a legacy sample that will allow us to compare results obtained in the optical and infrared wavelength regions. In GES iDR4 all observations for the listed cool benchmarks were completed, except for GJ 551 (Proxima Centauri), for which we will most probably have to rely on UVES archival data in future data releases.

4.3. Additional OBA benchmarks

While benchmark stars – with APs as independent as possible from spectroscopy – are becoming available for FGK and M types, as we discussed above, the situation is not as favourable in the case of hotter stars. This is due to the lack of interferometric data and the lack of spectrophotometry in the ultraviolet where the flux of these stars dominates. With this limitation in mind, one can, however, define a sample of well-studied A, B, and O-type stars with relatively well-established parameters in the refereed literature – even if not independent from spectroscopy.

For the calibration of APs of A-type stars, we selected 5 benchmark stars previously observed for the AP calibration of hot stars for Gaia (Bailer-Jones et al. 2013). These Gaia benchmark stars were observed with $S/N \approx 1000$, using the Hermes@Mercator ($R=85000$) in La Palma, Spain. Additional Gaia OBA benchmark spectra are being observed in ongoing dedi-

Table 6. List of OBA benchmark candidates observed by GES, none was analyzed in any internal release so far. A few more OBA stars will be observed before the end of the survey. Magnitudes and spectral types are from SIMBAD.

Star	V (mag)	Type	T_{eff} (K)	$\log g$ (dex)	Status
HD 93128 ^a	6.90	O3.5V	49 300	4.10	started
HD 319699 ^a	9.63	O5V	41 200	3.91	started
HD 163758 ^a	7.32	O6.5Iafp	34 600	3.28	observed
HD 68450 ^a	6.44	O9.7II	30 600	3.30	observed
τ Sco ^{b,c,d,e,f,g}	2.81	B0.2V	31 750	4.13	observed
θ Car ^{c,d}	2.76	B0Vp	31 000	4.20	observed
γ Peg ^{b,c,h}	2.84	B2IV	22 350	3.82	observed
HD 56613 ^c	7.21	B8V	13 000	3.92	observed
134 Tau ⁱ	4.87	B9IV	10 850	4.10	observed
68 Tau ^j	4.31	A2IV	9 000	4.00	observed

References for APs: (a) Holgado et al., in preparation (see text); (b) Nieva & Przybilla (2012); (c) Lefever et al. (2010); (d) Hubrig et al. (2008); (e) Simón-Díaz et al. (2006); (f) Mokiem et al. (2005); (g) Martins et al. (2012); (h) Morel & Butler (2008); (i) Smith & Dworetzky (1993); (j) Burkhardt & Coupry (1989).

cated observing programs. We complemented the set with one late B-type star with $T_{\text{eff}} \approx 11\,000$ K (134 Tau). These stars were carefully selected to cover different spectral subtypes, to have small $v \sin i$ values, and to be bright and visible from Paranal. Their optical spectra show sufficiently deep and narrow absorption lines in the wavelength regions also observed by GES. They are presently being observed by GES and will be used not only for survey-level homogenization, but also for testing the quality of APs and elemental abundance computed by the WG13 nodes, for all GES A- and late B-type stars in various Galactic young OCs.

For the early B-type stars, the selected pool of candidate benchmarks had their parameters (T_{eff} and $\log g$) estimated solely from high-resolution spectroscopic data (e.g., this excludes T_{eff} measurements based on photometric indices). Also, only studies treating the line formation in non-LTE were considered. The model atmospheres used may be either LTE or non-LTE (LTE being a reasonable assumption for B-type dwarfs; Przybilla et al. 2011), but a full line blanketing was considered a requirement. We performed a comparison of the available studies for each candidate B-type benchmark for GES, and rejected discrepant measurements (e.g., a few of the very high gravities from Daflon & Cunha 2004, and references therein). In some cases, stars were studied by various authors with similar data and methods, but we preferred one set over another to avoid redundancies. For example we used the results of Nieva & Przybilla (2012) for the four stars in common with Nieva & Simón-Díaz (2011), or for the three stars in common with Irrgang et al. (2014). The stars eventually selected have consistent APs from at least two high-quality and independent studies. It is important to note that most B stars analysed by GES, and generally belonging to young OCs, are fast rotators (e.g., $\langle v \sin i \rangle \sim 160$ km s⁻¹ in NGC 3293). On the contrary, the abundance studies in the literature are heavily biased against such objects. As a consequence, the vast majority of the selected B benchmark stars are slow rotators (by far the fastest rotator is θ Car with $v \sin i \sim 110$ km s⁻¹; Hubrig et al. 2008). This caveat should be kept in mind.

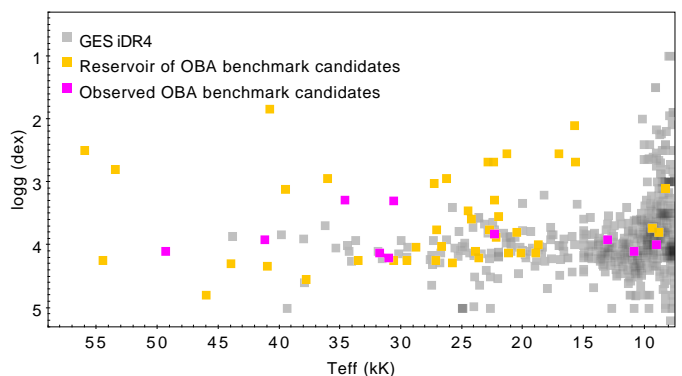


Fig. 9. Position of OBA benchmark candidates on the T_{eff} - $\log g$ plane. The OBA benchmarks are plotted as magenta squares; the pool of OBA benchmarks from which a few more will be selected for observations is represented by yellow squares; the GES iDR4 sample is reported in the background as grey squares.

The O-type candidate benchmarks were selected from the new Galactic O-Star Spectroscopic Survey spectral classification standard grid (Maíz Apellániz et al. 2015), which is a recent revision of the atlas for spectral classification, first established by Walborn & Fitzpatrick (1990). The full grid comprises more than 100 stars with spectral subtypes from O2 to O9.7 and luminosity classes from V to Ia, in both hemispheres, and it has been observed at high resolution ($R \approx 50\,000$) in two dedicated surveys (OWN and IACOB, see Barbá et al. 2010, 2014; Simón-Díaz et al. 2011b,c, 2015). A quantitative and homogeneous spectroscopic analysis of the OWN and IACOB samples is being performed within the framework of the IACOB project, and the results will soon be published (Holgado et al., in preparation), along with the full spectra library. The multi-epoch spectra of the OWN and IACOB projects also allow for variability searches, and a literature comparison with recent hot star surveys results for $v \sin i$, T_{eff} , $\log g$, and helium abundance (Repolust et al. 2004; Markova et al. 2014; Martins et al. 2015), is also being carried out.

Table 6 lists the OBA candidate benchmarks observed by GES up to now, while Figure 9 shows the parameter coverage of both the observed and candidate OBA benchmarks in the T_{eff} - $\log g$ plane. We expect to observe a few more OBA benchmarks before the end of the survey.

4.4. GES benchmarks results

Benchmark stars were used in GES iDR4 both within each WG to homogenize the results of different abundance analysis nodes (see, e.g. Smiljanic et al. 2014) and at the survey level to homogenize the results of different WGs (see H17). Additionally, in iDR4, the FGK benchmark stars are among the few calibrators that are also used to provide an external reference for APs, i.e., they are used as *absolute* calibrators. For example in WG11, they are used to define weights for each of the abundance analysis node results, that vary for different regions of the AP space based on that node results on benchmark stars. The calibration procedures derived using benchmarks, among other calibrators, are applied to all survey data and therefore it is useful to examine the effects of the whole process on the benchmark stars themselves. Figure 10 shows differences of the iDR4 recommended GES APs and $[\text{Fe}/\text{H}]$ values with the reference AP values (Heiter et al. 2015b) and NLTE metallicities (Jofré et al. 2014). The average differences are $T_{\text{eff}} = 14 \pm 113$ K, $\log g = -0.07 \pm 0.19$ dex, and

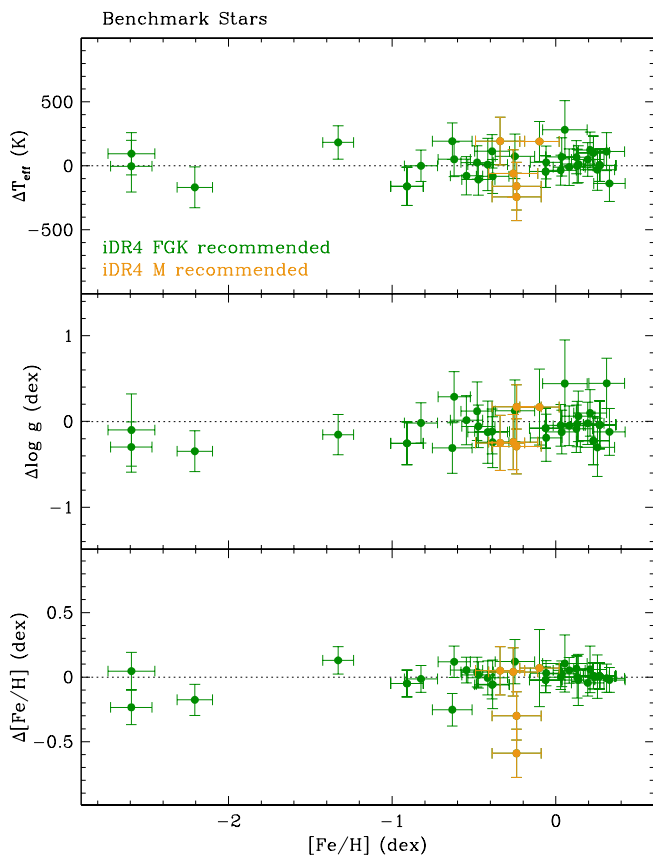


Fig. 10. Comparison of GES iDR4 recommended values with the reference APs (Heiter et al. 2015b) and $[\text{Fe}/\text{H}]$ (Jofré et al. 2014) values. In all panels, FGK benchmark stars are plotted in green and M benchmarks in orange. All differences are in the sense GES minus reference.

$[\text{Fe}/\text{H}] = -0.02 \pm 0.13$ dex. In all cases, the average offsets are negligible, and the dispersions give an idea of the typical GES performances on these high S/N ratio spectra.

5. Star clusters

Often, the goal of providing astrophysical calibrations for a spectroscopic survey is achieved by observing clusters in the MW. Both relatively old OCs (Section 5.1), and GCs (Section 5.3) are used in various surveys (RAVE, GALAH, and APOGEE, for example). They are extremely powerful calibrators of both APs and abundance ratios, for a number of reasons:

- although their APs are not as accurate as those of benchmark stars (Section 4), clusters contain many stars with similar — to first order — distances, ages, and chemical compositions⁸; thus, clusters provide extremely robust calibrators, because they also provide a way to statistically estimate the *uncertainty* on determined metallicities and abundance ratios;
- both OCs and GCs can — globally — rely upon a vast literature of photometric, astrometric, and spectroscopic measurements, and on very advanced models of stellar structure

⁸ With caution on some light (C, N, O, Na, Mg) and s-process elements, which can vary significantly in GC stars (see, e.g., Gratton et al. 2012). Also, spreads in $[\text{Fe}/\text{H}]$ are observed or claimed in a few GCs. This needs to be duly taken into account when using these clusters as calibrators.

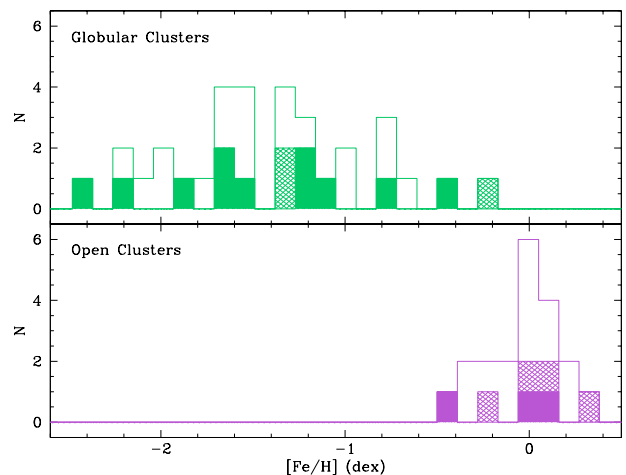


Fig. 11. Metallicity distribution of calibrating clusters: the top panel shows GCs and the bottom one OCs. Heavily shaded histograms show clusters included in iDR4; lightly shaded histograms the ones that will be included in future releases (see also Tables 8 and 7); empty histograms represent a pool of viable candidates to complete the coverage. A few of them could be selected in the next observing runs, depending on observations scheduling and data homogenization needs.

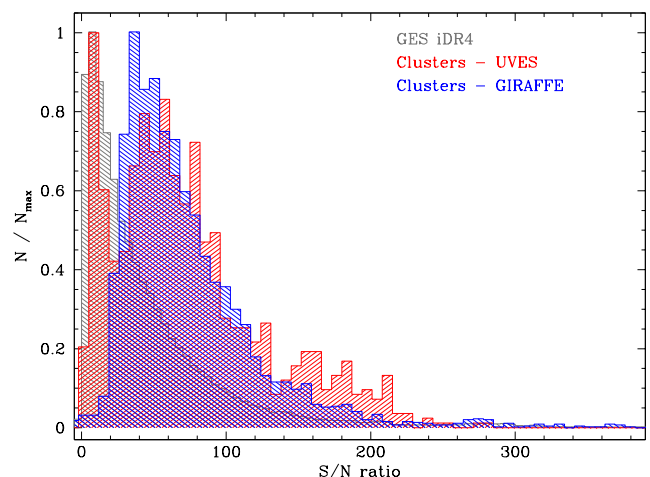


Fig. 12. S/N ratio of individual spectra of calibrating cluster stars, both in open and globular clusters. There are typically >3 exposures per star per setup. The required S/N ratio per star — after combining at least three spectra per star — was >50 , thus individual exposures peak roughly around 30–40 for GIRAFFE, who was driving the total exposure time. A tail of low S/N spectra for UVES contains mostly archival spectra of subgiants and MS stars.

and evolution, that are invaluable tools, making clusters ideal reference objects for both *external calibration* and *literature cross-checks*;

- having stars with virtually the same distance, it is possible to precisely know surface gravity, which is one of the most difficult quantities to derive for field stars without an absolute distance determination (see also Section 6); in general it is possible to derive precise APs from the many high-quality photometric catalogues available, thus clusters also provide an invaluable testbench for a survey’s APs determination;
- cluster stars have different APs, varying along the sequences of the colour-magnitude diagram in a regular way, allowing for the investigation of chemical abundance trends with pa-

Table 7. GES calibrating open clusters, with basic properties from Dias et al. (2002, and latest updates), and [Fe/H] metallicity from Heiter et al. (2014), except where noted. The status column refers only to the GES *calibration* observations, i.e., to those OCs that were observed with both the OC observing setups and the MW ones. The last column indicates other surveys using each OC as calibrator, along with other useful annotations.

Cluster	Dist (pc)	E(B–V) (mag)	Age (Gyr)	[Fe/H] (dex)	⟨RV⟩ (km/s)	Status	Notes
NGC 3532	492	0.028	0.30	+0.00	4.33	in iDR3	RAVE
NGC 6705 (M11)	1877	0.428	0.25	+0.12	35.08	in iDR3	internal calibrator
NGC 2243 ^a	2450	0.060	4.00	−0.48	59.84	in iDR3/4	APOGEE
Melotte 71	3154	0.113	0.24	−0.27	0.55	observed	RAVE, APOGEE
NGC 6253	1510	0.200	5.00	+0.34	−29.40	observed	very metal-rich
NGC 2420	2480	0.040	2.00	−0.05	73.57	observed	APOGEE
NGC 2477	1300	0.240	0.60	+0.07	7.26	started	RAVE, GALAH

^(a)Distance, reddening, and age from Bragaglia & Tosi (2006).

rameters: *no other calibrator allows for this kind of check of the internal consistency of an abundance analysis*, which is invaluable even for each individual method, even before comparing different methods;

- finally, the AP variations of cluster stars — having the same metallicity — allows for a very efficient *internal calibration* of a complex survey like GES; in particular, they allow the linking of various abundance analysis techniques employed by the many GES abundance analysis nodes concerning giants and dwarfs, cool and hot stars, GIRAFFE and UVES spectra.

Star clusters in iDR4 were not used as absolute (external) calibrators like benchmark stars, but were rather used *a posteriori* to verify the quality of the whole homogenization procedure at the node, WG, and survey levels (see also Section 5.5). The metallicity range covered by GES calibrating clusters is presented in Figure 11, while Figure 12 shows the distribution of S/N ratios for individual spectra, where typically each star was observed three times per setup.

5.1. OC selection criteria

Calibrating OCs⁹ were selected to interface with other current spectroscopic surveys, including also well known and studied clusters, to cover the metallicity range of interest. In the case of OCs, however, we tried to use as much as possible the targets selected by the GES OC group, because they already gather state-of-the-art literature data in terms of photometry, membership, binarity, and so on (see Bragaglia et al., in preparation, for more details), and because we could profit from the GES analysis to further select more reliable members. This is also the reason why calibrating OC observations started later in the survey than GC ones.

We gave priority to relatively old OCs, where a red clump is present¹⁰, so that in many calibrating OCs we will have both red clump giants and main sequence dwarfs. The GES science target OCs are generally observed with the UVES 580 setup, and the GIRAFFE HR15N and HR9B setups (see Table 1). Additionally, the stars selected for calibrations were also observed with the HR10 and HR21 GIRAFFE setups, i.e., those used for MW field

⁹ We term *calibrating OCs* here the OCs (or OC stars) that are observed specifically for the purpose of calibration, i.e., with both the MW field setups and the OC setups. Many more OC stars and OCs are observed for GES scientific purposes, and they will be called *science OCs*. Generally, the calibrating OC stars are a subset of the science OCs.

¹⁰ In any case, we did not select OCs younger than 100–200 Myrs as calibrators.

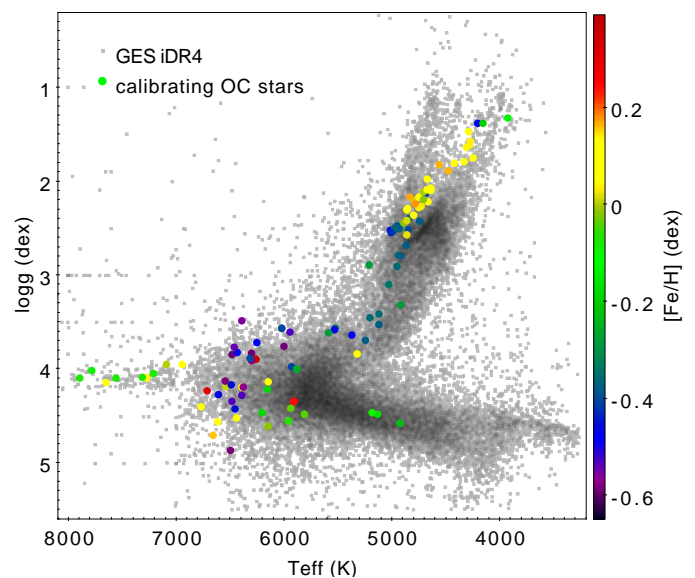


Fig. 13. Position on the T_{eff} - $\log g$ plane of the stars in calibrating OCs including archival data analyzed in iDR4 (namely NGC 2243, NGC 6705, and NGC 3532) and coloured according to their [Fe/H]. These stars were observed with both the MW field and the OC setups, there are of course many more OC stars observed with the OC setups only (of the order of 20 000, see Table 1). The whole GES iDR4 sample is reported in the background as smaller grey dots.

stars. This was intended to facilitate the internal calibration and to increase the wavelength coverage, thus making the abundance analysis of calibrating stars more robust.

In iDR4, three OCs were observed, as indicated in Table 7, while four more were completed recently. Additional OCs may be added in the future, depending on scheduling and analysis requirements.

5.2. Selection criteria for individual OC stars

For OCs, the individual star selection criteria varied from case to case. The reliable members observed with both the OC and field setups, and included in iDR4, are displayed in Figure 13. Our main guidelines were:

- to profit from the target selection effort performed by the GES OC group (Bragaglia et al., in preparation), selecting the candidates among stars that already had good membership information from the literature, or from previous GES internal releases; in other words, for most calibrating OCs,

Table 8. GES calibrating globular clusters, with basic properties from the Harris Galactic GC catalogue (Harris 1996, 2010), except where noted. The status column specifies the processing cycle in which each GC was analysed for the first time (see Section 2), and the last column indicates other surveys using each GC as calibrator, along with other useful annotations.

Cluster	[Fe/H] (dex)	E(B–V) (mag)	(m–M) _V (mag)	⟨RV⟩ (km/s)	σ ₀ (km/s)	Status	Notes
NGC 1851	–1.18	0.02	15.47	320.5	10.4	in iDR1	GALAH
NGC 4372	–2.17	0.39	15.03	72.3	3.9 ^a	in iDR1	metal-poor
NGC 5927	–0.49	0.45	15.82	–107.5	5.1 ^a	in iDR1	metal-rich
NGC 2808	–1.14	0.22	15.59	101.6	13.4	in iDR2	well studied
NGC 7078 (M 15)	–2.37	0.10	15.39	–107.0	13.5	in iDR2	APOGEE, GALAH
NGC 4833	–1.85	0.32	15.08	200.2	3.9 ^a	in iDR2	metal-poor
NGC 6752	–1.54	0.02	13.13	–26.7	4.9	in iDR3	RAVE, GALAH
NGC 104 (47 Tuc)	–0.72	0.04	13.37	–18.0	11.0	in iDR3/4	GALAH
NGC 362	–1.26	0.05	14.83	223.5	6.4	in iDR4	GALAH
NGC 1904 (M 79)	–1.60	0.01	15.59	205.8	5.3	in iDR4	well studied
NGC 7089 (M 2)	–1.65	0.06	15.50	–5.3	8.2	in iDR4	APOGEE
NGC 6553	–0.18	0.63	15.83	–3.2	6.1	observed	metal-rich
NGC 1261	–1.27	0.01	16.09	68.2	...	observed	well studied
NGC 6218 (M 12)	–1.37	0.19	14.01	–41.4	4.5	observed	RAVE

^(a)Radial velocity dispersion from Lardo et al. (2015).

the selected stars are a subsample of those observed for scientific purposes;

- to connect stars in different evolutionary phases, i.e., on the red clump and on the MS, whenever it was possible to select MS stars in a convenient magnitude range without including too many fast rotating stars in the sample;
- to sample a range of APs to test the self-consistency of the abundance analysis – similarly to the case of GCs – selecting stars in a range of 1–2 mag on the MS for those OCs for which a low fraction of fast rotators were present in the affordable magnitude ranges; in those OCs, we selected stars spanning a range of 1–2 magnitudes;

Additionally, ESO FLAMES archival data of the relevant OCs will be included in GES, as explained above: for example, many of the stars analysed in NGC 6705 or M 67 come from the ESO UVES archive. It is important to note that scientific OC observations can also be used by the WGs or by WG15 to homogenize the results.

5.3. GC selection criteria

The selection of calibrating GCs¹¹ proceeded by considering clusters that were used by other surveys like RAVE (Steinmetz et al. 2006; Zwitter et al. 2008; Siebert et al. 2011; Lane et al. 2011), GALAH (De Silva et al. 2015, Martell, 2014, private communication), and APOGEE (Frinchaboy et al. 2012, 2013; Anders et al. 2013; Mészáros et al. 2013), or that were subject to numerous high-resolution studies in the past.

Another fundamental criterion was the availability of wide field ($\approx 25'$, the FLAMES field of view), accurate photometric data in the literature or in the archives. Unfortunately, at the time when GES started, not many public photometric catalogues were available that covered the required field of view. Therefore, we made use of the large amount of WFI (Wide Field Imager) public GC data in the ESO archive. All relevant data were pre-reduced with IRAF and then analyzed with DAOPHOT II and ALLSTAR (Stetson 1987, 1992), and the resulting magnitudes will be published in the next public GES release. A more comprehensive

¹¹ GCs are not part of the scientific targets of GES, they are only observed for calibration purposes.

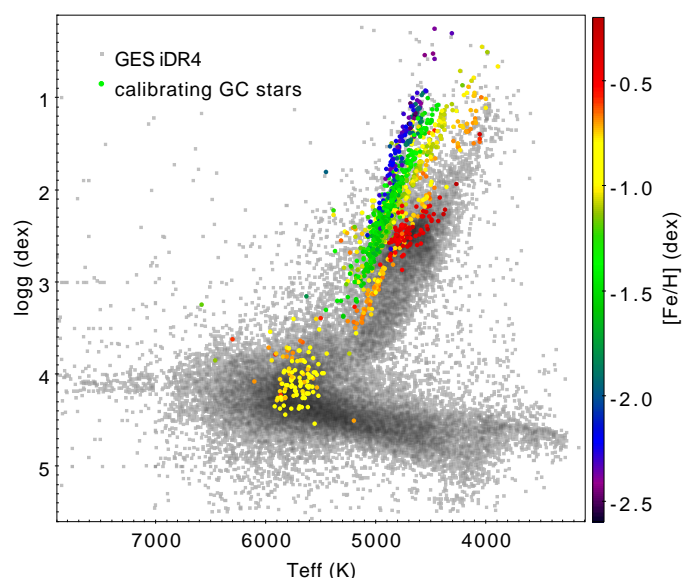


Fig. 14. Position on the T_{eff} - $\log g$ plane of selected member stars in calibrating GCs, including archival data analyzed in iDR4 and coloured according to their [Fe/H]. The whole GES iDR4 sample is reported in the background as smaller grey squares.

set of photometric catalogues, including data from all available public archives, is being prepared by P. Stetson¹² and the catalogues for GES GCs will be published elsewhere. It is important to stress that for dense stellar fields like GCs, the available survey catalogues – used to select GES targets for the MW field – are not precise enough. An example of the improvement that specific crowded-field PSF-fitting techniques can bring over a standard photometric analysis was presented by An et al. (2008) concerning GCs in SDSS.

We thus created a sample including as many clusters as possible, selected from the other surveys calibrating samples, that were visible from the South. We then filled the gaps in [Fe/H] with clusters having public photometry data (from the

¹² <http://www3.cadc-ccda.hia-ihp.nrc-cnrc.gc.ca/en/community/STETSON/homogeneous/>

ESO archive or from the literature). Special care was taken in including metal-rich GCs, as an interface with the OCs (see next Section) and considering that the majority of GES field targets are relatively metal-rich.

Twelve GCs were analyzed in iDR4, but two of them were not complete: NGC 4372 and NGC 6553. They will be fully included in subsequent releases, along with a few more GCs. A complete list of observed GCs can be found in Table 8, with the metallicity coverage illustrated in Figure 11.

5.4. Selection criteria for individual GC stars

We focused on red giants, because they are generally the best-studied objects in the literature. A few subgiants and main sequence (MS) stars were previously observed with UVES or GIRAFFE and were included in the GES analysis cycles along with other relevant ESO archival data. For UVES, we avoided repeating stars that already had good-quality UVES spectra in the archive. We did however repeat with UVES a few of the stars having GIRAFFE observations in the archive, to build a small sample of stars observed with both instruments for internal calibration purposes. All the other UVES targets were high probability members, based on their position in the CMD¹³. Stars with companions brighter than 1% of their flux in a 1' circle were excluded from observations.

For GIRAFFE, we gave highest priority to red giants having already archival observations in non-GES HR setups (see Table 1), because (i) they were in most cases analyzed and published, so we had additional information like RVs and chemistry to assess their membership and (ii) having a larger wavelength coverage (with more GIRAFFE setups observed) can produce a more reliable estimate of the APs and abundance ratios. Some effort was dedicated, whenever possible, to observe a few stars in common with other spectroscopic surveys mentioned above. Whenever additional membership information was available in the literature (RVs, proper motions, metallicities), it was used to select the most probable cluster members.

Depending on the GC and on the available body of archival data, the final sample of stars analyzed in iDR4 per GC was of the order of 10–50 with UVES and 50–200 with GIRAFFE. All GES data were observed with UVES 580 and GIRAFFE HR10 and HR21. The candidates and archival data span a range of 1–3 magnitudes along the red giant branch in each GC, which implies significant variations of APs in stars with the same [Fe/H], thus allowing for rather precise tests on the parameters and the self-consistency of the analysis (see below). To select provisional members for this paper, we used a 3σ cut around the median RV and [Fe/H] of the GES iDR4 recommended values, that were always fully compatible with the literature reference values reported in Table 8. The position in the theoretical $T_{\text{eff}}\text{-log } g$ plane of the selected members can be seen in Figure 14.

¹³ During the first few GES runs, due to strict scheduling requirements, we were forced to observe three clusters with high differential reddening: NGC 4833, NGC 5927, and NGC 4372. For these, the percentage of member stars among the selected targets was significantly lower than for the other GCs. For NGC 5927 we could rely on a published study with RVs of red clump stars (Simmerer et al. 2013), therefore in that case the majority of selected stars turned out to be members. Anyway, even if field contaminants cannot directly help for calibrations, they have an obvious scientific value for GES.

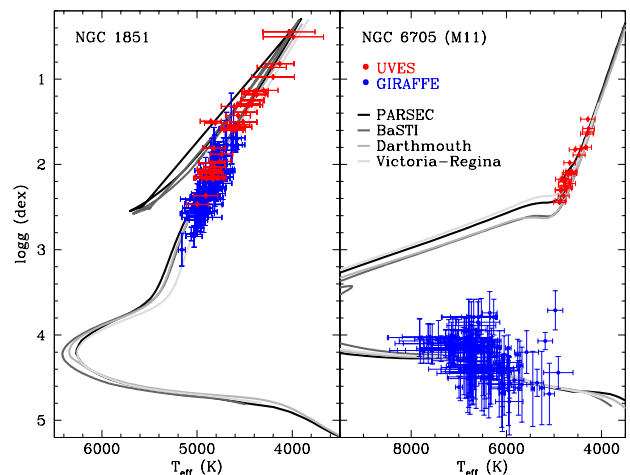


Fig. 15. Example of comparison with theoretical models for NGC 1851 and NGC 6705 (M 11). All stars observed in NGC 6705 are plotted, even those that are observed only with the OC setups. UVES targets are plotted in red and GIRAFFE ones in blue. Four different sets of isochrones are plotted (see text for more details) as thick lines of different colours.

5.5. Selected results on calibrating clusters

Clusters were used within GES past releases at many different levels, to compare results obtained by different nodes, WGs, or observing setups, and to study internal trends of abundances with APs. They were useful to identify various problems that were later remedied in iDR4. Clusters were not, however, used as *absolute* calibrators in iDR4, but rather were used *a posteriori* to test the goodness of the overall homogenization process. Therefore it is interesting to compare the final iDR4 cluster recommended values with state-of-the-art external reference values, to give an idea of the results of the whole GES homogenization procedure.

A first comparison can be made with stellar models. In Figure 15 we show NGC 1851 and NGC 6705 as an example. A more extensive discussion and set of model comparisons will be presented in H17. We used four different sets of stellar isochrones: the PARSEC set (Bressan et al. 2012; Chen et al. 2014; Tang et al. 2014); the BaSTI set (Pietrinferni et al. 2004, 2006); the Dartmouth set (Dotter et al. 2008); and the Victoria-Regina set (VandenBerg et al. 2006). We adopted the parameters listed in Tables 7 and 8, with an age of 12.8 Gyr for NGC 1851. As can be seen, apart from the small residual offset between the GIRAFFE and UVES results (see below), the GES iDR4 recommended parameters agree well with theoretical predictions, within the quoted uncertainties. Considering the automated analysis, which is not tailored to obtain the best results for GCs, this is a very satisfactory result.

For a different comparison, we computed independent T_{eff} and $\log g$ values from our photometry, described in Section 5.3, using the Alonso et al. (1999) and Alonso et al. (1996) calibrations for giants and dwarfs, respectively. To obtain T_{eff} , we used the B–V and V–K colors, dereddened with the E(B–V) values listed in Tables 8 and 7, and we transformed the $K_{2\text{MASS}}$ magnitudes into K_{TCS} ones with the relations by Ramírez & Meléndez (2005). Similarly, we obtained $\log g$ using bolometric corrections from the cited calibrations and fundamental relations. We assumed a fixed mass of $0.8 M_{\odot}$ for evolved GC stars and a

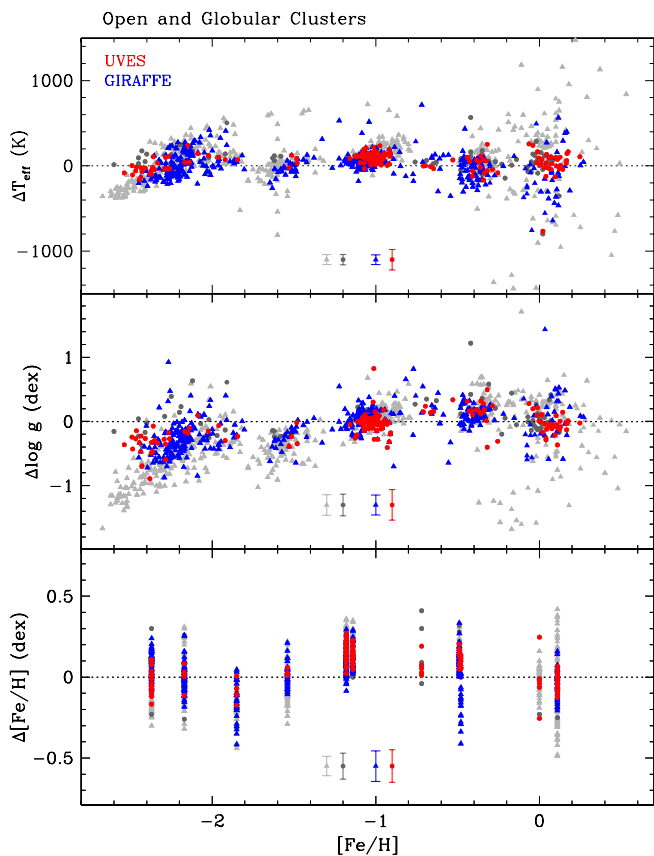


Fig. 16. Difference between the GES recommended APs and $[\text{Fe}/\text{H}]$ and the photometric reference APs and literature $[\text{Fe}/\text{H}]$ (see text for more details). The GES iDR4 results are plotted as blue triangles (for GIRAFFE) and red circles (for UVES). Greyed out symbols represent the previous internal release (iDR2 + iDR3) corresponding values. The top panels shows ΔT_{eff} as a function of GES $[\text{Fe}/\text{H}]$, the middle panel $\Delta \log g$ as a function of GES $[\text{Fe}/\text{H}]$, and the bottom panel $\Delta[\text{Fe}/\text{H}]$ as a function of the literature reference $[\text{Fe}/\text{H}]$. The median internal errors of GES recommended values are also plotted at the center of each panel.

varying mass for OC stars at various evolutionary stages, based on the above selected isochrone sets.

The results of the comparison are presented in Figure 16, where we also show the results obtained during the previous internal processing cycle (iDR2 + iDR3, based on data gathered in the first two years of GES observations). As can be seen, there has been enormous improvement from the previous to the present internal data release, especially at the two extremes of the metallicity range. The causes of the improvement lie in the cyclic nature of GES data analysis and calibration, where with each cycle not only new data are added, but new procedures are introduced either to implement lessons learned in previous cycles, or to refine the quality control and data analysis. A similar analysis, based on the entire GES sample, will be presented in Randich et al. (2016, in preparation)

The median iDR4 offsets to the reference values are always compatible with zero – within the uncertainties – and the typical 1σ spreads for both UVES and GIRAFFE are compatible with the median GES errors. Of course, the selected reference parameters depend on the chosen reference cluster parameters in Tables 8 and 7, on the colour-temperature calibration relations and their errors, on the accuracy and precision of the reference

photometry, and so on. Had we chosen the (González Hernández & Bonifacio 2009) colour-temperature calibration, for example, the median T_{eff} differences reported below would have been lower by about ≈ 60 K. What is important to note here is that the reference APs are derived with an independent method and yet the agreement is quite satisfactory, especially considering that cluster stars in GES are analyzed with the same method as field stars, i.e., without profiting from the extra information on distance provided by clusters. For UVES we obtained $\langle \Delta T_{\text{eff}} \rangle = 71 \pm 93$ K, $\langle \Delta \log g \rangle = 0.04 \pm 0.18$ dex, and $\langle \Delta[\text{Fe}/\text{H}] \rangle = 0.06 \pm 0.11$ dex. For GIRAFFE we obtained $\langle \Delta T_{\text{eff}} \rangle = -49 \pm 149$ K, $\langle \Delta \log g \rangle = -0.21 \pm 0.30$ dex, and $\langle \Delta[\text{Fe}/\text{H}] \rangle = 0.00 \pm 0.16$ dex, where the quoted uncertainties are 1σ spreads.

6. Asteroseismologic constraints

The resonant frequencies of stochastically-driven pulsators (such as the Sun and other FGK-type dwarfs and giants with turbulent convective envelopes) allow for precise estimates of stellar APs that are largely independent of spectroscopy (see e.g. Miglio et al. 2013, and references therein). As an example the surface gravity $\log g$, a relatively difficult quantity to measure directly from spectroscopy alone, is strongly correlated with the frequency at maximum oscillation power (ν_{max}):

$$\nu_{\text{max}} \propto g / \sqrt{T_{\text{eff}}}$$

(Brown 1991; Kjeldsen & Bedding 1995; Belkacem et al. 2011). Given the typical accuracy of these scaling relations and the precision of the measured ν_{max} , the seismic estimates of $\log g$ are likely more precise ($\sigma_{\log g} \sim 0.05$ dex) than those derived from standard spectroscopic methods, that are typically in the range $\sigma_{\log g} \approx 0.1 - 0.2$ dex. Note also the weak dependence of $\log g$ on T_{eff} : a shift in T_{eff} of ≈ 100 K leads to an expected variation in $\log g$ of less than 0.01 dex, at least in the mass range covered by GES.

There is good agreement between the $\log g$ values inferred from seismology and from classical methods for bright stars spanning a wide range of effective temperature and evolutionary state (dwarfs, sub-giants and red giants, Morel & Miglio 2012; Morel et al. 2014). This supports the application of scaling relations in deriving weakly model-dependent $\log g$ estimates, at least for the tested domains of metallicity and surface gravity. In the case of Kepler, the spectroscopic and seismic gravities have shown a good agreement, with no evidence of systematic offsets: $\langle \log g_{\text{spec}} - \log g_{\text{seism}} \rangle = +0.08 \pm 0.07$ dex for dwarfs (Bruntt et al. 2012) and -0.05 ± 0.30 dex for giants (Thygesen et al. 2012). Fixing $\log g$ to the seismic value in spectroscopic analysis — whenever possible — has become an increasingly popular technique (e.g., Huber et al. 2013). The availability of precise seismic $\log g$ estimates for thousands of solar-like pulsators detected by CoRoT (Michel et al. 2008) and Kepler (Borucki et al. 2010) missions makes them valuable targets for science verification and/or calibration.

6.1. Asteroseismic collaborations with GES

GES observed selected targets in the LRC01 and LRA01 CoRoT fields (in the Galactic center and anticenter directions, respectively) where CoRoT has detected and characterized more than 2000 oscillating G-K red giants (Mosser et al. 2010, see also Figure 17). More than 1500 red giants were observed with the GES field setups (Table 1) and analysed in iDR4. A subset of a few tens of the candidates, for which the oscillation spectra

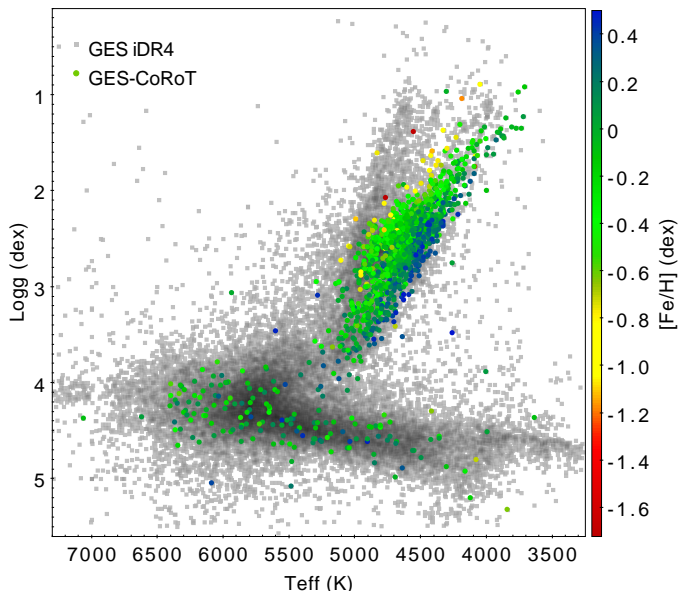


Fig. 17. Position in the T_{eff} - $\log g$ plane of the GES targets – in the direction of the CoRoT center and anti-center fields – that were analyzed in iDR4, coloured according to their $[\text{Fe}/\text{H}]$. The GES iDR4 analysis is not the final result, because the GES-CoRoT project is still ongoing (see text for more details). The whole GES iDR4 sample is reported in the background as smaller grey squares.

have also allowed to derive their evolutionary state (either RGB or central He-burning, Mosser et al. 2011), were observed with UVES. The GES-CoRoT collaboration will provide a set of reference parameters to compare with the GES recommended parameters, similarly to what was done by Jofré et al. (2014) for the benchmark stars. The final reference APs for these stars will be derived by a combined team of GES and CoRoT scientists, after an iterative process: the spectroscopic T_{eff} value obtained by GES and the seismic parameter ν_{max} will provide a first seismic $\log g$ value, which will be held fixed in the following spectroscopic analysis by a subset of the GES abundance analysis nodes participating to the GES-CoRoT project. The new T_{eff} value will then provide a new seismic $\log g$ estimate, and so on, until convergence (typically no more than two iterations are needed). The results of this project will be presented elsewhere.

Similarly, thousands of solar-like oscillating giant stars have been discovered in Campaigns 1 and 3 of the K2 mission. GES observations are currently planned for a combined asteroseismic-spectroscopic analysis using individual resonant frequencies with the Birmingham asteroseismic group, allowing for far more insight on the physics of stellar interiors than what is available using simple scaling relations (e.g., Davies et al. 2016). Other spectroscopic surveys are targeting giants observed by Kepler and CoRoT for similar purposes, so a large sample of overlapping spectroscopic observations is expected (see also Figure 18), allowing for future survey intercalibrations. More details on the target selection strategy, data analysis, and use of these calibrators for the intercalibration with other surveys can be found in Gilmore et al., (2016, in preparation).

7. Discussion and conclusions

The GES calibration and data analysis strategy is designed to take care of the internal consistency and the overall robustness of its results with respect to literature or reference values. The abundance analysis process in GES is complex, resulting from

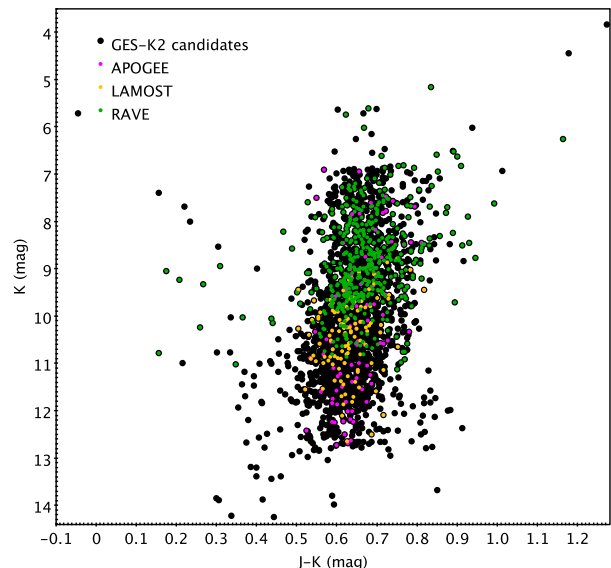


Fig. 18. Kepler red giants in the K2 C1 and C3 fields, that were selected as candidates for GES observations (large black circles). Stars already observed by other surveys are highlighted in different colors (APOGEE in magenta, LAMOST in yellow, and RAVE in green).

observations of different objects with different instrumental setups, and analyzed by several abundance analysis nodes, using virtually all of the existing state-of-the-art techniques. While this is one of the major strengths of the GES data analysis, it requires particular attention in the process of data homogenisation, that produces the GES recommended RVs, APs, and chemical abundance ratios.

Different classes of calibrating objects were selected, with the main goals of covering the different observational setups, the AP space covered by the GES scientific targets, and the variety of methods used to analyze them. In particular, we selected a sample of 31 RV standards from the Gaia RV standards catalogue (Soubiran et al. 2013); a pool of star clusters, both GCs and OCs, either used as calibrators by other major ongoing surveys or well studied in the literature, of which 21 were observed to date; a list of FGK benchmark stars in common with the Gaia list of benchmarks (Heiter et al. 2015b) was observed, complemented by cooler M benchmarks and OBA candidate benchmark stars; and a list of thousands of targets in common with those of the two major asteroseismic space missions, CoRoT and Kepler, was also observed. In a few cases the calibration planning of GES and its requirements have spawned calibration projects like the Gaia benchmarks spectroscopic project (Blanco-Cuaresma et al. 2014; Jofré et al. 2014, 2015; Hawkins et al. 2016) or the GES-CoRoT collaboration, that will prove useful for many other projects and surveys.

The complex GES calibration and homogenization procedures, described in Smiljanic et al. (2014), Lanzafame et al. (2015), and H17, are applied at different levels of the data processing (node, WG, and survey-wide) and they are applied to all the GES targets (field stars, OC scientific targets, and calibrators). Therefore, it is particularly instructive to examine the outcome of the whole calibration process on the calibrating objects themselves. We presented a few examples of the comparisons that are routinely performed in GES. In particular, we showed how the cyclic processing leads to significant improvement from

cycle to cycle. We also quantitatively showed that the agreement between GES iDR4 recommended values and reference values for the calibrating objects are very satisfactory. The average offsets and spreads are generally compatible with the GES measurement errors, proving that the performance goals set by Gilmore et al. (2012) and Randich et al. (2013) are being met.

Acknowledgements. Based on data products from observations made with ESO Telescopes at the La Silla Paranal Observatory under programme ID 188.B-3002 and 193.B-0936. These data products have been processed by the Cambridge Astronomy Survey Unit (CASU) at the Institute of Astronomy, University of Cambridge, and by the FLAMES/UVES reduction team at INAF-Osservatorio Astrofisico di Arcetri. These data have been obtained from the Gaia-ESO Survey Data Archive, prepared and hosted by the Wide Field Astronomy Unit, Institute for Astronomy, University of Edinburgh, which is funded by the UK Science and Technology Facilities Council. This work was partly supported by the European Union FP7 programme through ERC grant number 320360 and by the Leverhulme Trust through grant RPG-2012-541. We acknowledge the support from INAF and Ministero dell'Istruzione, dell'Università e della Ricerca (MIUR) in the form of the grant "Premiale VLT 2012". The results presented here benefit from discussions held during the Gaia-ESO workshops and conferences supported by the ESF (European Science Foundation) through the GREAT Research Network Programme. S.F. and T.B. acknowledge the support from the New Milky Way project funded by a grant from the Knut and Alice Wallenberg foundation. C.L. gratefully acknowledges financial support from the European Research Council (ERC-CoG-646928, Multi-Pop, PI: N. Bastian). U.H. and A.J.K. acknowledge support from the Swedish National Space Board (Rymdstyrelsen). The research of A.L. been subsidized by the Belgian Federal Science Policy Office under contract No. BR/143/A2/BRASS. R.S. acknowledges support by the National Science Center of Poland through grant 2014/15/B/ST9/03981. C.A.P. is thankful for support from the Spanish Ministry of Economy and Competitiveness (MINECO) through grant AYA2014-56359-P. J.M. acknowledges support from the ERC Consolidator Grant funding scheme (project STARKEY, G.A. n.615604). T.M. acknowledges financial support from Belspo for contract PRODEX GAIA-DPAC. S.G.S. acknowledges the support by Fundação para a Ciência e Tecnologia (FCT) through national funds and a research grant (project ref. UID/FIS/04434/2013, and PTDC/FIS-AST/7073/2014). S.G.S. also acknowledge the support from FCT through Investigador FCT contract of reference IF/00028/2014 and POPH/FSE (EC) by FEDER funding through the program "Programa Operacional de Factores de Competitividade – COMPETE". L.S. acknowledges support by the Ministry of Economy, Development, and Tourism's Millennium Science Initiative through grant IC120009, awarded to The Millennium Institute of Astrophysics (MAS). M.Z. acknowledges support by the Ministry of Economy, Development, and Tourism's Millennium Science Initiative through grant IC120009, awarded to The Millennium Institute of Astrophysics (MAS), by Fondecyt Regular 1150345 and by the BASAL CATA PFB-06. E.J.A. and M.T.C. acknowledge the financial support from the Spanish Ministerio de Economía y Competitividad, through grant AYA2013-40611-P. S.Z. acknowledge the support from the INAF grant "PRIN INAF 2014", "Star won't tell their ages to Gaia, Galactic Archaeology with wide-area asteroseismic". This research has made use of the WEBDA database, operated at the Department of Theoretical Physics and Astrophysics of the Masaryk University; of the TOP-CAT catalogue handling and plotting tool (Taylor 2005); of the Simbad database and the VizieR catalogue access tool, CDS, Strasbourg, France (Ochsenbein et al. 2000); and of NASA's Astrophysics Data System.

References

Adelman, S. J., White, R. E., & Pyper, D. M. 1980, *ApJS*, 43, 491
 Alonso, A., Arribas, S., & Martínez-Roger, C. 1996, *A&A*, 313, 873
 Alonso, A., Arribas, S., & Martínez-Roger, C. 1999, *A&AS*, 140, 261
 An, D., Johnson, J. A., Clem, J. L., et al. 2008, *ApJS*, 179, 326
 Anders, F., Chiappini, C., Santiago, B. X., et al. 2013, arXiv:1311.4549
 Anthony-Twarog, B. J., & Twarog, B. A. 2000, *AJ*, 119, 2282
 Bailer-Jones, C. A. L., Andrae, R., Arcay, B., et al. 2013, *A&A*, 559, A74
 Balcells, M., Bann, C. R., Carter, D., et al. 2010, *Proc. SPIE*, 7735, 77357G
 Ballester, P., Modigliani, A., Boitquin, O., et al. 2000, *The Messenger*, 101, 31
 Barbá, R. H., Gamen, R., Arias, J. I., et al. 2010, *Revista Mexicana de Astronomía y Astrofísica Conference Series*, 38, 30
 Barbá, R., Gamen, R., Arias, J. I., et al. 2014, *Revista Mexicana de Astronomía y Astrofísica Conference Series*, 44, 148
 Barden, S. C., Jones, D. J., Barnes, S. I., et al. 2010, *Proc. SPIE*, 7735, 773509
 Barrado y Navascués, D., Deliyannis, C. P., & Stauffer, J. R. 2001, *ApJ*, 549, 452
 Belkacem, K., Goupil, M. J., Dupret, M. A., et al. 2011, *A&A*, 530, AA142
 Bensby, T., Feltzing, S., & Oey, M. S. 2014, *A&A*, 562, AA71

Bertaux, J. L., Lallement, R., Ferron, S., Boonne, C., & Bodichon, R. 2014, *A&A*, 564, AA46
 Bikmaev, I. F., Ryabchikova, T. A., Bruntt, H., et al. 2002, *A&A*, 389, 537
 Blanco-Cuaresma, S., Soubiran, C., Jofré, P., & Heiter, U. 2014, *A&A*, 566, AA98
 Bland-Hawthorn, J., Krumholz, M. R., & Freeman, K. 2010, *ApJ*, 713, 166
 Boyajian, T. S., von Braun, K., van Belle, G., et al. 2012, *ApJ*, 757, 112
 Borucki, W. J., Koch, D., Basri, G., et al. 2010, *Science*, 327, 977
 Bragaglia, A., & Tosi, M. 2006, *AJ*, 131, 1544
 Bressan, A., Marigo, P., Girardi, L., et al. 2012, *MNRAS*, 427, 127
 Brown, T. M. 1991, *ApJ*, 371, 396
 Bruntt, H., Basu, S., Smalley, B., et al. 2012, *MNRAS*, 423, 122
 Burkhardt, C., & Coupry, M. F. 1989, *A&A*, 220, 197
 Carraro, G., Girardi, L., & Marigo, P. 2002, *MNRAS*, 332, 705
 Chen, Y., Girardi, L., Bressan, A., et al. 2014, *MNRAS*, 444, 2525
 Chubak, C., Marcy, G., Fischer, D. A., et al. 2012, arXiv:1207.6212
 Crowther, P. A., Lennon, D. J., & Walborn, N. R. 2006, *A&A*, 446, 279
 Daffon, S., & Cunha, K. 2004, *ApJ*, 617, 1115
 Davies, G. R., Silva Aguirre, V., Bedding, T. R., et al. 2016, *MNRAS*, 456, 2183
 de Bruijne, J. H. J. 2012, *Ap&SS*, 341, 31
 de Jong, R. S., Barden, S., Bellido-Tirado, O., et al. 2014, *Proc. SPIE*, 9147, 91470M
 de Laverny, P., Recio-Blanco, A., Worley, C. C., & Plez, B. 2012, *A&A*, 544, AA126
 De Silva, G. M., Freeman, K. C., Bland-Hawthorn, J., et al. 2015, *MNRAS*, 449, 2604
 Demory, B.-O., Ségransan, D., Forveille, T., et al. 2009, *A&A*, 505, 205
 De Pascale, M., Worley, C. C., de Laverny, P., et al. 2014, *A&A*, 570, AA68
 Dias, W. S., Alessi, B. S., Moitinho, A., & Lépine, J. R. D. 2002, *A&A*, 389, 871
 Donati, P., Cantat Gaudin, T., Bragaglia, A., et al. 2014, *A&A*, 561, AA94
 Dotter, A., Chaboyer, B., Jevremović, D., et al. 2008, *ApJS*, 178, 89
 Ekström, S., Georgy, C., Eggenberger, P., et al. 2012, *A&A*, 537, AA146
 Freeman, K., & Bland-Hawthorn, J. 2002, *ARA&A*, 40, 487
 Frinchaboy, P. M., Thompson, B., Jackson, K. M., et al. 2013, *ApJ*, 777, L1
 Frinchaboy, P. M., Allende Prieto, C., Beers, T. C., et al. 2012, *American Astronomical Society Meeting Abstracts* #219, 219, #428.04
 Gaia Collaboration 2016, arXiv:1609.04153
 Gaia Collaboration, Brown, A. G. A., Vallenari, A., et al. 2016, arXiv:1609.04172
 Gilmore, G., Randich, S., Asplund, M., et al. 2012, *The Messenger*, 147, 25
 González Hernández, J. I., & Bonifacio, P. 2009, *A&A*, 497, 497
 Gratton, R. G., Carretta, E., & Bragaglia, A. 2012, *A&A Rev.*, 20, 50
 Gray, R. O., Graham, P. W., & Hoyt, S. R. 2001, *AJ*, 121, 2159
 Guarcello, M. G., Prisinzano, L., Micela, G., et al. 2007, *A&A*, 462, 245
 Guarcello, M. G., Micela, G., Peres, G., Prisinzano, L., & Sciortino, S. 2010, *A&A*, 521, AA61
 Gustafsson, B., Edvardsson, B., Eriksson, K., et al. 2008, *A&A*, 486, 951
 Harris, W. E. 1996, *AJ*, 112, 1487
 Harris, W. E. 2010, arXiv:1012.3224
 Heiter, U., Soubiran, C., Netopil, M., & Paunzen, E. 2014, *A&A*, 561, A93
 Heiter, U., Lind, K., Asplund, M., et al. 2015a, *Phys. Scr*, 90, 054010
 Heiter, U., Jofré, P., Gustafsson, B., et al. 2015b, *A&A*, 582, A49
 Hill, G. M. 1995, *A&A*, 294, 536
 Hawkins, K., Jofre, P., Heiter, U., et al. 2016, arXiv:1605.08229
 Huber, D., Chaplin, W. J., Christensen-Dalsgaard, J., et al. 2013, *ApJ*, 767, 127
 Hubrig, S., Briquet, M., Morel, T., et al. 2008, *A&A*, 488, 287
 Irrgang, A., Przybilla, N., Heber, U., et al. 2014, *A&A*, 565, AA63
 Jackson, R. J., Jeffries, R. D., Lewis, J., et al. 2015, *A&A*, 580, A75
 Jeffries, R. D., Maxted, P. F. L., Oliveira, J. M., & Naylor, T. 2006, *MNRAS*, 371, L6
 Jeffries, R. D., Jackson, R. J., Cottaar, M., et al. 2014, *A&A*, 563, AA94
 Jofré, P., Heiter, U., Soubiran, C., et al. 2014, *A&A*, 564, AA133
 Jofré, P., Heiter, U., Soubiran, C., et al. 2015, *A&A*, 582, A81
 Kassim, M., Janes, K. A., Friel, E. D., & Phelps, R. L. 1997, *AJ*, 113, 1723
 Kjeldsen, H., & Bedding, T. R. 1995, *A&A*, 293, 87
 Koposov, S. E., Gilmore, G., Walker, M. G., et al. 2011, *ApJ*, 736, 146
 Kordopatis, G., Gilmore, G., Steinmetz, M., et al. 2013, *AJ*, 146, 134
 Lane, R. R., Kiss, L. L., Lewis, G. F., et al. 2011, *A&A*, 530, A31
 Lanzafame, A. C., Frasca, A., Damiani, F., et al. 2015, *A&A*, 576, A80
 Lardo, C., Pancino, E., Bellazzini, M., et al. 2015, *A&A*, 573, AA115
 Lebzelter, T., Seifahrt, A., Utenthaler, S., et al. 2012, *A&A*, 539, AA109
 Lefever, K., Puls, J., Morel, T., et al. 2010, *A&A*, 515, AA74
 Lindgren, L., & Perryman, M. A. C. 1996, *A&AS*, 116, 579
 Lindgren, S., Heiter, U., & Seifahrt, A. 2016, *A&A*, 586, A100
 Luck, R. E. 1994, *ApJS*, 91, 309
 Maíz Apellániz, J., Alfaro, E. J., Arias, J. I., et al. 2015, *Highlights of Spanish Astrophysics VIII*, 603
 Majewski, S. R., Schiavon, R. P., Frinchaboy, P. M., et al. 2015, arXiv:1509.05420
 Markova, N., Puls, J., Simón-Díaz, S., et al. 2014, *A&A*, 562, A37

- Martins, F., Escolano, C., Wade, G. A., et al. 2012, *A&A*, 538, AA29
- Martins, F., Hervé, A., Bouret, J.-C., et al. 2015, *A&A*, 575, A34
- Mészáros, S., Holtzman, J., García Pérez, A. E., et al. 2013, *AJ*, 146, 133
- Michel, E., Baglin, A., Auvergne, M., et al. 2008, *Science*, 322, 558
- Miglio, A., Chiappini, C., Morel, T., et al. 2013, *European Physical Journal Web of Conferences*, 43, 03004
- Mignard, F. 2005, *Astrometry in the Age of the Next Generation of Large Telescopes*, 338, 15
- Modigliani, A., Mulas, G., Porceddu, I., et al. 2004, *The Messenger*, 118, 8
- Mokiem, M. R., de Koter, A., Puls, J., et al. 2005, *A&A*, 441, 711
- Morel, T., & Butler, K. 2008, *A&A*, 487, 307
- Morel, T., & Miglio, A. 2012, *MNRAS*, 419, L34
- Morel, T., Miglio, A., Lagarde, N., et al. 2014, *A&A*, 564, AA119
- Mosser, B., Belkacem, K., Goupil, M.-J., et al. 2010, *A&A*, 517, AA22
- Mosser, B., Barban, C., Montalbán, J., et al. 2011, *A&A*, 532, AA86
- Neves, V., Bonfils, X., Santos, N. C., et al. 2014, *A&A*, 568, AA121
- Newberg, H. J., Carlin, J. L., Chen, L., et al. 2012, *Galactic Archaeology: Near-Field Cosmology and the Formation of the Milky Way*, 458, 405
- Nieva, M.-F., & Simón-Díaz, S. 2011, *A&A*, 532, AA2
- Nieva, M.-F., & Przybilla, N. 2012, *A&A*, 539, AA143
- Ochsenbein, F., Bauer, P., & Marcout, J. 2000, *A&AS*, 143, 23
- Önehag, A., Heiter, U., Gustafsson, B., et al. 2012, *A&A*, 542, AA33
- Pasquini, L., Avila, G., Allaert, E., et al. 2000, *Proc. SPIE*, 4008, 129
- Pasquini, L., Brucalassi, A., Ruiz, M. T., et al. 2012, *A&A*, 545, A139
- Pietrinferni, A., Cassisi, S., Salaris, M., & Castelli, F. 2004, *ApJ*, 612, 168
- Pietrinferni, A., Cassisi, S., Salaris, M., & Castelli, F. 2006, *ApJ*, 642, 797
- Przybilla, N., Nieva, M.-F., & Butler, K. 2011, *Journal of Physics Conference Series*, 328, 012015
- Ramírez, I., & Allende Prieto, C. 2011, *ApJ*, 743, 135
- Ramírez, I., & Meléndez, J. 2005, *ApJ*, 626, 446
- Randich, S., Gilmore, G., & Gaia-ESO Consortium 2013, *The Messenger*, 154, 47
- Repolust, T., Puls, J., & Herrero, A. 2004, *A&A*, 415, 349
- Rojas-Ayala, B., Covey, K. R., Muirhead, P. S., & Lloyd, J. P. 2012, *ApJ*, 748, 93
- Sacco, G. G., Morbidelli, L., Franciosini, E., et al. 2014, *A&A*, 565, 113
- Searle, S. C., Prinja, R. K., Massa, D., & Ryans, R. 2008, *A&A*, 481, 777
- Siebert, A., Williams, M. E. K., Siviero, A., et al. 2011, *AJ*, 141, 187
- Simmerer, J., Feltzing, S., & Primas, F. 2013, *A&A*, 556, A58
- Simón-Díaz, S., Herrero, A., Esteban, C., & Najarro, F. 2006, *A&A*, 448, 351
- Simón-Díaz, S. 2010, *A&A*, 510, AA22
- Simón-Díaz, S., Castro, N., Herrero, A., et al. 2011, *Journal of Physics Conference Series*, 328, 012021
- Simón-Díaz, S., Castro, N., Garcia, M., Herrero, A., & Markova, N. 2011, *Bulletin de la Societe Royale des Sciences de Liege*, 80, 514
- Simón-Díaz, S., Garcia, M., Herrero, A., Maíz Apellániz, J., & Negueruela, I. 2011, *Stellar Clusters & Associations: A RIA Workshop on Gaia*, 255
- Simón-Díaz, S., Negueruela, I., Maíz Apellániz, J., et al. 2015, *Highlights of Spanish Astrophysics VIII*, 576
- Smiljanic, R., Korn, A. J., Bergemann, M., et al. 2014, *A&A*, 570, AA122
- Smith, K. C., & Dworetsky, M. M. 1993, *A&A*, 274, 335
- Soubiran, C., Jasniewicz, G., Chemin, L., et al. 2013, *A&A*, 552, A64
- Sousa, S. G., Santos, N. C., Adibekyan, V., et al. 2014, *A&A*, 561, AA21
- Steinmetz, M., Zwitter, T., Siebert, A., et al. 2006, *AJ*, 132, 1645
- Stetson, P. B. 1987, *PASP*, 99, 191
- Stetson, P. B. 1992, *Astronomical Data Analysis Software and Systems I*, 25, 297
- Taylor, M. B. 2005, *Astronomical Data Analysis Software and Systems XIV*, 347, 29
- Tang, J., Bressan, A., Rosenfield, P., et al. 2014, *MNRAS*, 445, 4287
- Thompson, H. M. A., Keenan, F. P., Dufton, P. L., et al. 2008, *MNRAS*, 383, 729
- Thygesen, A. O., Frandsen, S., Bruntt, H., et al. 2012, *A&A*, 543, AA160
- Valentini, M., Morel, T., Miglio, A., Fossati, L., & Munari, U. 2013, *European Physical Journal Web of Conferences*, 43, 03006
- VandenBerg, D. A., Bergbusch, P. A., & Dowler, P. D. 2006, *ApJS*, 162, 375
- Villanova, S., Randich, S., Geisler, D., Carraro, G., & Costa, E. 2010, *A&A*, 509, AA102
- von Braun, K., Boyajian, T. S., Kane, S. R., et al. 2011, *ApJ*, 729, LL26
- von Braun, K., Boyajian, T. S., Kane, S. R., et al. 2012, *ApJ*, 753, 171
- Walborn, N. R., & Fitzpatrick, E. L. 1990, *PASP*, 102, 379
- Worley, C. C., de Laverny, P., Recio-Blanco, A., et al. 2012, *A&A*, 542, AA48
- Yadav, R. K. S., Bedin, L. R., Piotto, G., et al. 2008, *A&A*, 484, 609
- Zwitter, T., Siebert, A., Munari, U., et al. 2008, *AJ*, 136, 421
- 1 INAF – Osservatorio Astrofisico di Arcetri, Largo E. Fermi 5, 50125 Firenze, Italy, e-mail: pancino@arcetri.inaf.it
- 2 ASI Science Data Center, Via del Politecnico s/n, 00133 Roma
- 3 Astrophysics Research Institute, Liverpool John Moores University, 146 Brownlow Hill, Liverpool L3 5RF, United Kingdom
- 4 INAF – Osservatorio Astronomico di Bologna, Via Ranzani 1, 40127 Bologna, Italy
- 5 INAF – Osservatorio Astronomico di Roma, Via Frascati 33, 00040, Monte Porzio Catone, Roma, Italy
- 6 Space Telescope Science Institute, 3700 San Martin Drive, Baltimore, MD 21218, US
- 7 Instituto de Astrofísica, Pontificia Universidad Católica de Chile, Av. Vicuña Mackenna 4860, 782-0436 Macul, Santiago, Chile
- 8 Millennium Institute of Astrophysics, Av. Vicuña Mackenna 4860, 782-0436 Macul, Santiago, Chile
- 9 Dipartimento di Fisica e Astronomia, Alma Mater Studiorum, Università di Bologna, Viale Berti Pichat 6/2, 40127, Bologna, Italy
- 10 Department of Physics and Astronomy, Uppsala University, Box 516, SE-751 20 Uppsala, Sweden
- 11 Institute of Astronomy, University of Cambridge, Madingley Road, Cambridge CB3 0HA, United Kingdom
- 12 Royal Observatory of Belgium, Ringlaan 3, 1180, Brussels, Belgium
- 13 Institut d'Astrophysique et de Géophysique, Université de Liège, Allée du 6 Août, Bât. B5c, 4000 Liège, Belgium
- 14 Instituto de Astrofísica de Canarias, E-38200 La Laguna, Tenerife, Spain
- 15 Departamento de Astrofísica, Universidad de La Laguna, E-38205 La Laguna, Tenerife, Spain
- 16 Laboratoire d'astrophysique de Bordeaux, Univ. Bordeaux, CNRS, B18N, allé Geoffroy Saint-Hilaire, 33615 Pessac, France
- 17 Dipartimento di Fisica e Astronomia, Università di Padova, Vicolo dell'Osservatorio 2, 35122 Padova, Italy
- 18 Leibnitz Institute für Astrophysics (AIP), An der Sternwarte 16, 14482 Potsdam, Germany
- 19 Observatoire de Genève, Université de Genève, CH-1290 Versoix, Switzerland
- 20 Núcleo de Astronomía, Facultad de Ingeniería, Universidad Diego Portales, Av. Ejercito 441, Santiago, Chile
- 21 GEPI, Observatoire de Paris, PSL Research University, CNRS, Univ. Paris Diderot, Sorbonne Paris Cité, 5 Place Jules Janssen, 92190 Meudon, France
- 22 Lund Observatory, Department of Astronomy and Theoretical Physics, Box 43, SE-221 00 Lund, Sweden
- 23 Research School of Astronomy & Astrophysics, Australian National University, Cotter Road, Weston Creek, ACT 2611, Australia
- 24 Centre for Astrophysics Research, STRI, University of Hertfordshire, College Lane Campus, Hatfield AL10 9AB, United Kingdom
- 25 Astrophysics Group, Research Institute for the Environment, Physical Sciences and Applied Mathematics, Keele University, Keele, Staffordshire ST5 5BG, United Kingdom
- 26 INAF - Osservatorio Astronomico di Palermo, Piazza del Parlamento 1, 90134, Palermo, Italy
- 27 INAF - Padova Observatory, Vicolo dell'Osservatorio 5, 35122 Padova, Italy
- 28 Instituto de Astrofísica de Andalucía-CSIC, Apdo. 3004, 18080, Granada, Spain
- 29 Institute of Astronomy, University of Edinburgh, Blackford Hill, Edinburgh EH9 3HJ, United Kingdom
- 30 Dipartimento di Fisica e Astronomia, Sezione Astrofisica, Università di Catania, via S. Sofia 78, 95123, Catania, Italy
- 31 Nicolaus Copernicus Astronomical Center, Polish Academy of Sciences, ul. Bartycka 18, 00-716, Warsaw, Poland
- 32 Institut d'Astronomie et d'Astrophysique, Université libre de Bruxelles, Boulevard du Triomphe, 1050 Brussels, Belgium
- 33 Instituto de Física y Astronomía, Universidad de Valparaíso, Chile
- 34 INAF - Osservatorio Astrofisico di Catania, via S. Sofia 78, 95123, Catania, Italy
- 35 Departamento de Ciencias Físicas, Universidad Andres Bello, Republica 220, Santiago, Chile
- 36 European Southern Observatory, Alonso de Cordova 3107 Vitacura, Santiago de Chile, Chile
- 37 Instituto de Astrofísica e Ciências do Espaço, Universidade do Porto, CAUP, Rua das Estrelas, 4150-762 Porto, Portugal
- 38 Physics Department, Lancaster University, Lancaster LA1 4YB, UK
- 39 UPJV, Université de Picardie Jules Verne, 33 Rue St Leu, F-80080 Amiens, France